Quantitative paleoecology in shallow-marine settings: The value of ostracods and foraminifers from the Holocene North Adriatic record

# Quantitative paleoecology in shallow-marine settings: the value of ostracods and foraminifers from the Holocene North Adriatic record

Journal: Palaeogeography, Palaeoclimatology, Palaeoecology

Authors: Giulia Barbieri[a]*, Veronica Rossi[a], Stefano Claudio Vaiani[a], Utsha Dasgupta[b], Alessandro Amorosi[a]

[a] Department of Biological, Geological and Environmental Sciences, University of Bologna, Via Zamboni 67, 40126, Bologna, Italy

[b] Department of Geological Sciences, Jadavpur University, Kolkata 700032, India

* corresponding author; e-mail: giulia.barbieri21@unibo.it; postal address: Department of Biological, Geological and Environmental Sciences, University of Bologna, Via Zamboni 67, 40126, Bologna, Italy

Additional e-mail addresses: V.R.: veronica.rossi4@unibo.it; S.C.V.: stefano.vaiani@unibo.it; U.D.: utshadasgupta93@gmail.com; A.A.: alessandro.amorosi@unibo.it.

**Keywords**

Sequence stratigraphy; Po Delta; prodelta; micropaleontology

## Abstract

Benthic ostracods and foraminifers are commonly applied as paleoenvironmental indicators in shallow marine successions, ignoring that individual meiofaunal groups could provide distinct information. We aim to shed light on the distinct paleoecological record of benthic ostracods and foraminifers by analyzing the shallow marine Holocene succession of the Po Delta (Italy) in a sequence stratigraphic fashion. Multivariate elaborations connecting the modern North Adriatic reference set to fossil data allowed to investigate community dynamics, obtain quantitative estimates of (paleo-)environmental drivers and assess the

meiofaunal response to coastal and delta dynamics through time and space under the influence of allogenic and autogenic factors. Benthic ostracods and foraminifers easily discern transgressive (TST) and highstand (HST) systems tract, and also discriminate between locations at different distance from paleo-river mouths under highstand conditions. Specifically, community changes reflecting shifts in delta regimes at distal locations suggest that lobe-fringe deposits are more indicated for paleoenvironmental purposes. We emphasize that a deep knowledge of the analyzed datasets should drive the interpretation of multivariate outputs, as reconstructed values from significantly similar deposits could be inappropriate, and the lack of true modern analogs could reflect authentic differences in community composition, or either pitfalls in the modern reference set. Our results show that ostracods evidence depositional regimes determined by the interplay of sediment supply and hydrodynamic energy in relationship with the position from main river outlets; on the other hand, foraminifers highlight changes in riverine inputs in terms of organic matter. Our findings demonstrate that shallow marine benthic ostracods and foraminifers provide distinct but complementary paleoecological information, and their integration allows to achieve high-resolution reconstructions.

## 1. Introduction

Ostracods and foraminifers represent a main component of the marine benthos (Murray, 2006; Horne et al., 2012; Yasuhara et al., 2017). Characterized by similar size ranges (from a few microns to millimeters), short life cycles and mostly possessing calcareous hard shells that ensure high preservation potential in the sedimentary record, they form abundant communities on the seafloor (Gooday, 2001; Schellenberg, 2007).

Nevertheless, the taxonomic positions of benthic ostracods (multicellular crustaceans) and foraminifers (unicellular protistans) highlight remarkable biological and paleoecological differences. Benthic ostracods swim relatively fast (a few $cm \cdot s^{-1}$), whereas foraminifers move very slowly (a few $\mu m \cdot s^{-1}$) or can even be sessile (Murray, 2001; Sutherland et al., 2011). Although benthic ostracods can be subject to long-distance transport due to natural events or anthropogenic activities (Faasse, 2013; Tanaka et al., 2018), the lack of a nauplius larval stage determines a low dispersal potential (Rodriguez-Lazaro and Ruiz-Muñoz, 2012). Conversely, the

45 global distribution of propagules banks was hypothesized to explain the greater dispersion of benthic
46 foraminifers even in coastal settings (Weinmann and Goldstein, 2017). Concerning the growing mechanism,
47 ostracods perform several moults and discarded valves are preserved in the sediment, whereas benthic
48 foraminifers mainly add successive chambers on single tests (Mesquita-Joanes et al., 2012; Hohenegger, 2018).
49 Other biological differences, such as reproduction mechanisms and feeding strategies, could account for
50 distinct structure and composition of assemblages (Yasuhara et al., 2012).

51 Comparing the (paleo-)ecological response of benthic ostracods and foraminifers may shed new light on the
52 interaction among species, community patterns and environmental parameters, especially in shallow-marine
53 areas, where the interplay of many environmental factors may lead to high temporal and spatial heterogeneity.
54 Since the application of the meiofauna as paleoecological indicator is rooted in the principle of taxonomic
55 uniformitarianism, the micropaleontological investigation of past shelves dynamics should ideally start from
56 modern reference datasets. Unfortunately, heterogeneity in measured parameters and taxonomic resolution
57 has commonly prevented the development of integrated meiofaunal distribution models. Studies performed
58 on Mediterranean shelves mostly deal with single groups (e.g., Goineau et al., 2015; Sciuto et al., 2015; Benito
59 et al., 2016) and the few works performed on both benthic ostracods and foraminifers aimed to identify
60 ecological patterns in response to anthropogenic pressure (e.g., Triantaphyllou et al., 2005; Pascual et al., 2008;
61 Salvi et al., 2015). As a consequence, even though benthic ostracods and foraminifers have been extensively
62 employed in late Quaternary paleoenvironmental reconstructions (e.g., Carboni et al., 2002; Flaux et al., 2013;
63 Cacciari et al., 2019), paleoecological information has been extracted from separate modern datasets (e.g.,
64 Breman, 1975; Jorissen, 1988; Mendes et al., 2004; Frezza and Carboni, 2009; Frezza and Di Bella, 2015) and
65 reviews (e.g., Athersuch et al., 1989; Murray, 2006; Horne et al., 2012). An integrated analysis of present-day
66 benthic ostracods and foraminifers performed on the North Adriatic river-influenced shelf (Barbieri et al., 2019)
67 revealed that these two groups have distinct distribution patterns driven by specific environmental factors (i.e.,
68 bathymetry, substrate grain-size and organic-matter fluxes). The distribution model could serve as a basis to

investigate and quantify the response of shallow-marine benthic communities to allogenic (sea-level oscillations) or autogenic (e.g., delta lobe switching) factors acting on river-influenced shelves. The well-constrained chronostratigraphic framework of its inland counterpart (Ciabatti, 1967; Stefani and Vincenzi, 2005; Amorosi et al., 2017; Campo et al., 2017; Giacomelli et al., 2018; Amorosi et al., 2019) makes the Po Delta-North Adriatic system an excellent venue where to analyze and weight up the response of benthic ostracod and foraminifer communities to deposition dynamics across the Holocene. Although some paleoenvironmental studies integrated marine benthic ostracods and foraminifers from upper Quaternary shallow-marine successions of the Mediterranean area (Amorosi et al., 2008; Fanget et al., 2013, 2016; Angue Minto'o et al., 2016), a critical comparison of these groups has never been performed.

In the present work, we describe and compare the vertical distribution patterns of benthic ostracods and foraminifers throughout the shallow-marine deposits of three cores from the Po Delta area along a N-S oriented transect, crossing two adjacent ancient delta lobes (Fig. 1). Specifically, we frame meiofauna quantitative data within two well-recognized sediment units: (i) the transgressive systems tract (TST), formed during the Holocene transgression, and (ii) the highstand systems tract (HST), deposited in response to deltaic progradation of two delta lobes (Volano and Goro) that were governed by distinct sediment dynamics under overall high progradation rates (Amorosi et al., 2020). We investigate the analogies with the modern North Adriatic benthic ostracod and foraminifer biofacies and quantitatively estimate trends in selected environmental parameters through the application of multivariate elaborations. Finally, we extract specific paleoecological indications from the two benthic groups, with the objective of comparing their resolution potential in fossil shelves subject to defined coastal and delta dynamics through time and space.

## 2. Stratigraphic and geomorphological framework

The Holocene sedimentary succession of the Po delta plain, developed on top of upper Pleistocene continental deposits, was formed in response to relative sea-level rise (Amorosi et al., 2017). The lower TST (9.5-8.5 cal kyr B.P.) consists of back-barrier deposits that mark the landward migration of a wave-dominated

93 estuarine system (Bruno et al., 2017). Above a wave ravinement surface, the upper TST (8.5-7.0 cal kyr B.P.)
94 includes a deepening-upward succession of transgressive barrier sands and offshore muds that represent the
95 deepest conditions within the entire Holocene succession (Amorosi et al., 2008). The boundary between
96 offshore and overlying prodelta facies (maximum flooding surface, MFS) records the turnaround from back-
97 stepping (TST) to prograding (HST) depositional systems, which took place in response to relative sea-level
98 stabilization (Amorosi et al., 2019), around 8-7 kyr B.P. (Vacchi et al., 2016). Stratigraphic condensation at the
99 MFS (Scarponi et al., 2017) was associated to persistently low accumulation rates, as clastic input was trapped
100 at the head of the estuary (Amorosi et al., 2019). Due to its poor lithological expression, the MFS has been
101 defined by the maximum value of the ratio between open-marine and fluvial-influenced benthic foraminifers,
102 and by ostracods shifts towards assemblages with predominant taxa tolerant to salinity oscillations (e.g.,
103 Amorosi and Colalongo, 2005; Amorosi et al., 2008).

104 Thick prodelta clays (up to ca. 20 m) capped by delta front sands record a complex pattern of coastal
105 progradation under highstand conditions (Amorosi et al., 2020). Steps in delta progradation were controlled by
106 distributary-channel avulsions and by the interplay with longshore currents. Geomorphological (i.e., preserved
107 sand ridges; Fig. 1), historical and archeological data indicate that one of the oldest wave-influenced (arcuate)
108 deltas in the northern coastal plain was fed by the Po di Ariano (the present-day Po di Goro) in the Early Roman
109 Age (Ciabatti, 1967; Fig. 1). Towards the south, the Volano lobe mostly prograded from the Roman to the Early
110 Medieval Age (Ciabatti, 1967; Correggiari et al., 2005a). In the second half of the 12th century (800-750 cal yr
111 B.P.), the Ficarolo river avulsion shifted the Po in a northern position. The increased activity of the Goro branch
112 caused the rapid outbuilding of a cuspate Po delta lobe, up to the XVI century, whereas the Volano river mouth
113 remained relatively stable (Ciabatti, 1967). Later, the Fornaci branch (the modern Po di Levante, Fig. 1) became
114 the main outlet and formed the first lobate delta of the Po River, marking the onset of the Modern-Age delta
115 characterized by several supply-dominated lobes prograding at rates even >100 m $yr^{-1}$(Correggiari et al.,
116 2005a).

Modern prodelta lobes show comparable size to their inland buried counterparts, with thickness up to ca. 15 m and lateral extension of 10-20 km. Their stratigraphic relations reflect activity of individual river branches during the last centuries (Correggiari et al., 2005a, 2005b).

## 3. Materials and methods

### *3.1 Experimental design and data collection*

Micropaleontological analyses were performed on Holocene shallow-marine deposits from three cores (Fig. 1) drilled by wire-line perforation in the southern portion of the modern Po Delta plain. Cores 187S4 (44°57'49" N, 12°15'09" E), EM13 (44°51'50" N, 12°17'05" E) and 205S9 (44°46'71" N, 12°15'05" E) are 35-54 m long and were specifically selected with approximately north-south orientation, in order to capture along-strike paleoecological variations across two adjacent lobes (i.e., Volano and Goro) with documented activity in historical times. Specifically, cores 187S4 and 205S9 were recovered in proximity to distributary channels, whereas core EM13 is located far from river mouths (Fig. 1). Sedimentological features and concise paleontological characteristics have been illustrated by Amorosi et al. (2003, 2017) and Campo et al. (2017), whereas the benthic foraminifer distribution of core 205S9 is reported in Dasgupta et al. (2020). In this work, we present quantitative benthic ostracod and foraminifer data from cores 187S4 and EM13, along with the quantitative ostracod distribution from core 205S9, and provide novel multivariate elaborations. The stratigraphic model by Amorosi et al. (2020) and surficial geological map by Ciabatti (1967) were used as a geological framework to compare the record of benthic foraminifers and ostracods from distinct, locally outcropping, Holocene beach-ridge sediment bodies.

Micropaleontological assemblages were recovered from (i) TST barrier sands and offshore clays, and from (ii) the stratigraphically expanded HST of the Volano and Goro delta lobes. The chronologic framework relies on 14 published radiocarbon dates integrated with one sample from core 187S4 (Table 1), dated at the Korea Institute of Geoscience and Mineral Resources (KIGAM, Republic of Korea). Calibration of conventional $^{14}C$ ages

was performed with Oxcal 4.2 (Bronk Ramsey, 2009) using the IntCal13 and Marine13 curves (Reimer et al., 2013) and a ΔR value of 139 ± 28 yr (Langone et al., 1996).

A total of 258 sediment samples of approximately 100-150 g of dry weight (151 from core EM13, 58 from core 205S9 and 49 from core 187S4) were selected for micropaleontological analyses and treated following the standard procedure adopted in other reference works from the study area (e.g., Rossi and Vaiani, 2008). Samples were dried at 60 °C, soaked overnight in 10% $H_2O_2$, water-screened with a 63 μm sieve and dried again for > 8 hours. Samples including abundant, well preserved microfossils were dry-sieved at 125 μm and divided using a microsplitter. At least 300 benthic foraminifers and 100 ostracod valves (with carapaces considered as two valves) were counted from the >125 μm fraction, otherwise, all the tests or valves were considered. Both adult and juvenile ostracod valves with morphological characters sufficiently developed to perform an identification at species level were counted. Literature adopted for taxonomic identification and structure of meiofaunal matrices are reported in Text S1 and Table S1.

*3.2 Data matrices*

Microfossil data matrices were treated prior to the application of multivariate analyses, following specific criteria in order to keep the data comparable to the modern reference set based on total assemblages (Barbieri et al., 2019). Clearly transported freshwater and brackish water taxa were removed from the ostracod dataset and only samples including >20 valves were retained, in accordance with other works from marine settings (Azzarone et al., 2020; Barbieri et al., 2019; Bassetti et al., 2010; Cronin et al., 1999). Samples including <300 individuals were removed from the benthic foraminifer matrix. The contribution of the fragile agglutinated taxon *Eggerella scabra* was discarded. Selected taxa with similar ecological characteristics were gathered up to the genus level in order to reduce the dataset dispersion and taxa with relative abundance >5% in at least one sample were retained. We harmonized variables and taxonomic nomenclature in modern and fossil datasets, as reported in Table S2.

### *3.3 Multivariate analyses*

Fossil data were subject to the Hellinger transformation, i.e. the square root of the relative abundance was computed (Legendre and Gallagher, 2001). Then, multivariate analyses were separately performed on benthic ostracod and foraminifer matrices using the Euclidean distance in order to obtain the Hellinger distance, a measure recommended to detect community changes in short environmental gradients that gives low weights to rare species (Legendre and Gallagher, 2001; Legendre and De Cáceres, 2013).

The contribution of taxa to the composition of sample groups was assessed by means of a Euclidean-based similarity percentage analysis (SIMPER – Clarke, 1993) carried out on Hellinger-transformed data, whereas average values were derived from relative abundance data in order to produce more straightforward outputs.

Paleoecological conditions were assessed through the application of the analogue matching technique (AM; (Simpson, 2007). AM identifies the *k*-closest modern sites to each fossil assemblage, and the degree of analogy is estimated through the computation of dissimilarity values between each fossil and modern sample. Fossil assemblages were compared to the modern North Adriatic ostracod and foraminifer biofacies determined through quantitative thresholds of environmental parameters presented in Barbieri et al. (2019), synthetized in Table 2 (geographic distribution in Fig. 2). This comparison also allowed the interpretation of the paleoecological record in relation to the amount of riverine input and relative distance from the main feeding channel. A threshold value to determine whether fossil samples have an adequate counterpart in the modern reference set should be applied considering selected percentiles (up to $20^{th}$) of the distribution of modern dissimilarities (Simpson, 2007). We chose the $20^{th}$ percentile as a critical threshold to discriminate analog from non-analog samples. Although this is considered an adequate value (Jackson and Williams, 2004), it is a bit higher than those traditionally employed in other studies (Overpeck et al., 1985; Anderson et al., 1989). This threshold was selected due to intrinsic properties of the distance measure and heterogeneity of the ostracod datasets. Specifically, the Hellinger distance allows to manipulate percentage data (as expressed in the modern datasets) and produces optimal results when samples share variables with intermediate frequencies (Legendre

and Gallagher, 2001). Nevertheless, it locally emphasized taxonomic discrepancies (e.g., taxa not recorded in the modern dataset, Table S2), increasing the dissimilarity between fossil and modern datasets and leading us to choose the $20^{th}$ percentile as the threshold value for ostracods (Hellinger distance = 0.616). This value was also applied to benthic foraminifers (Hellinger distance = 0.520) to keep the data comparable. Where several modern analogs were found for a fossil assemblage, we retained the four modern samples with the lowest dissimilarity values.

The distance between cores and modern assemblages was visualized through a weighted Principal Coordinates Analysis (wPCoA), where core samples were passively plotted as trajectories in stratigraphic order onto the ordination space defined by modern assemblages. To further refine the paleoecological characterization, predicted values of environmental drivers on the distribution of modern North Adriatic assemblages (Barbieri et al., 2019) and the associated standard error were extracted from microfossil assemblages and plotted against core stratigraphy using a generalized additive model, as it is used automatically in the wPCoA computation (Goring et al., 2009; Oksanen et al., 2019).

All the statistical elaborations were carried out in the R environment (version 3.6.1; R Core Team, 2019) using the packages “vegan” (Oksanen et al., 2019), “analogue” (Simpson and Oksanen, 2020), “mgcv” (Wood, 2011), and “ggplot2” (Wickham, 2016) for graphical outputs, whereas the SIMPER analysis was performed with PAST (PAleontological STatistics; Hammer et al., 2001).

## 4. Results

*4.1.1 Composition of fossil ostracod assemblages and analogies with modern North Adriatic sites*

Relatively high dissimilarity values were recorded between fossil and modern ostracod datasets, mostly due to peak frequencies (>70%) of dominant taxa in fossil assemblages, in contrast to the relatively homogeneous modern North Adriatic communities (maximum relative abundances <55%; Barbieri et al., 2019). Moreover,

fossil ostracod assemblages displayed relatively high abundances of species not recorded in the modern fauna (Table S2).

The SIMPER routine performed on ostracods revealed an overall average dissimilarity of 0.64 (Table 3). *Leptocythere ramosa*, *Pontocythere turbida, Semicytherura incongruens, Loxoconcha* ex gr. *rhomboidea*, *Palmoconcha turbida* and other *Semicytherura* account for most of the differences (cumulative contribution >55%).

Abundant statistically significant analogs were found for ostracod assemblages of transgressive deposits. These are mostly represented by samples of the shallow, sediment-starved northern Adriatic shelf (biofacies O5, Table 2), updrift of the main sediment input from the Po River (Figs. 2–4, Table S3). Scattered modern analogs are represented by samples located at either lower (biofacies O4) or higher (biofacies O6) depths, in areas with low-moderate river input. The lowest Hellinger distance values of the entire database indicate high similarity between transgressive ostracod assemblages from the three cores (Fig. 5A, Table S4). Transgressive ostracod assemblages are composed of similar frequencies of *S. incongruens, Pontocythere turbida,* other *Semicytherura* and *Loxoconcha* ex gr. *rhomboidea* (Table 3), locally associated to *Sagmatocythere napoliana* and *Cytheretta* spp.

A relatively low number of significant modern analogs was detected for the Volano ostracod assemblages (Table 4). Specifically, the few significant modern analogs found in core 205S9 belong to biofacies O4, located along the northernmost or central Adriatic coasts, where low to moderate river input is recorded. A single sample (13 m core depth) was considered similar to a modern sample from deep-water relict sands (biofacies O6; Fig. 2). A larger number of fossil assemblages is represented by significant modern analogs in core EM13 (Table 4, Fig. 3). In the lower portion of core EM13, one sample at 23.69 m depth was significantly similar to a modern site of the sediment-starved shelf (biofacies O5). The upper part of the lobe includes relatively high amounts of significant modern analogs, represented by shallow-water, mid-Adriatic sites with moderate river input on either sandy (biofacies O4) or muddy bottoms (biofacies O2). A moderate dissimilarity (0.48, Table S4)

was recorded between the Volano ostracod assemblages of cores 205S9 and EM13, with *Pontocythere turbida, S. incongruens* and *Palmoconcha turbida* representing the most abundant species (Fig. 5A, Table 3).

Ostracod assemblages from the Goro lobe in core 187S4 are represented by abundant modern analogs along the shallow Adriatic coast, under moderate sediment supply (biofacies O4, subordinately biofacies O2; Fig. 4). Concerning the Goro lobe ostracods from core EM13 (Fig. 3), one sample at 12.27 m core depth was considered significantly similar to a modern site immediately south of the Po Delta, at shallow water depth on fine-grained sediment enriched in organic matter under high sediment supply (biofacies O1). Non-analog sites (i.e., the most similar sites, but exceeding the threshold value defined by the 20$^{th}$ percentile of modern dissimilarities) for this interval were attributed to samples from the same area (biofacies O1) or, occasionally, from a southern position on muddy substrates (biofacies O2). Ostracod assemblages from the Goro deposits were characterized by high dissimilarity (1.1, Fig. 5A), due to the dominance of *L. ramosa* in core EM13 (68.4% on average). On the other hand, the Goro sediments from core 187S4 show an ostracod composition with common *Pontocythere turbida*, *S. incongruens*, *Palmoconcha turbida*, associated with moderate frequencies of *Xestoleberis* spp. and *Loxoconcha* ex gr. *rhomboidea* (Table 3).

*4.1.2 Composition of fossil benthic foraminifer assemblages and analogies with modern North Adriatic sites*

Fossil and modern foraminifer datasets are taxonomically homogeneous, with a single taxon showing frequencies >5% in fossil samples, but not in modern ones (*Haynesina* spp.; Table S2).

The overall dissimilarity between sediment units from each core is 0.42, as revealed by the SIMPER analysis (Table 5). Most of the differences among sediment units from the three cores (>55%) were determined by *Ammonia parkinsoniana – Ammonia tepida*, *Aubignyna perlucida*, *Quinqueloculina* group, *Porosononion* ex gr. *granosum* and *Triloculina* ex gr. *trigonula*, representing the most abundant taxa.

Benthic foraminifer assemblages from transgressive deposits showed statistically significant analogs in the modern North Adriatic (Figs. 2-4, Table 4). Specifically, transgressive assemblages from cores 187S4 and 205S9

256 are significantly similar to modern sites along the Adriatic coast, north of the Po Delta, under negligible organic
257 matter inputs and strong longshore currents (biofacies F3; Table 2). On the other hand, many significant
258 modern analogs of EM13 transgressive benthic foraminifer assemblages occur on the Adriatic shelf at high
259 water depth (biofacies F5). Relatively low dissimilarity values were recorded between transgressive benthic
260 foraminifer assemblages (Fig. 5B, Table S4), due to similar frequencies of the most common taxa, namely the
261 *Quinqueloculina* group (Table S2), *Porosononion* ex gr. *granosum*, *Adelosina* spp. and *Textularia agglutinans*.
262 The higher dissimilarity of transgressive assemblages from core EM13 was determined by the higher
263 contribution of *Buccella granulata, Neoconorbina terquemi, Rosalina bradyi* and *Asterigerinata mamilla* (Table
264 5).

265 Benthic foraminifer assemblages from the Volano lobe show abundant significant modern analogs in core
266 205S9, whereas a lower number of significantly similar modern sites was detected from core EM13 (Figs. 2, 3).
267 In core 205S9, between 25.25 and 23.50 m core depths, significantly similar modern sites are mostly located on
268 the shallow northern Adriatic coast with low organic matter levels (biofacies F3) and subordinately south of the
269 Po Delta on substrates with moderate organic matter (biofacies F2). Upwards, significant modern analogs are
270 positioned along the mid-Adriatic coast (biofacies F2) or in proximity of the Po and Adige delta outlets
271 (biofacies F1) under moderate to high organic matter inputs, respectively. In core EM13, up to 21.06 m core
272 depth, the Volano lobe shows a low number of significant modern analog sites along the northern and middle
273 Adriatic coasts (biofacies F3, F2). In the upper portion of the lobe, benthic foraminifers show high similarity to
274 modern sites in proximity or south of the Po and Adige delta mouths (biofacies F1, F2). The Volano benthic
275 foraminifer assemblages show a moderate dissimilarity between locations (0.39, Fig. 5B, Table S4), mostly
276 driven by the lower frequency of *A. parkinsoniana – A. tepida* in core EM13, associated to relatively high
277 concentrations of *A. perlucida, Porosononion* ex gr. *granosum* and *Quinqueloculina* group (Table 5).

278 A large number of significant analogs was found for benthic foraminifer assemblages from the Goro lobe
279 (Figs. 3, 4). Significantly similar modern analog sites for core 187S4 were identified along the shallow mid-

Adriatic coast (biofacies F2) or near the Po and Adige river mouths (biofacies F1) under moderate to high organic matter fluxes, with alternating trends along the prodelta succession. Oscillations in modern analogs were also detected for assemblages of core EM13, but with a dominance of significantly similar sites from the central Adriatic coast (biofacies F2). A very low dissimilarity (0.24; Fig. 5B, Table S4) was recorded between benthic foraminifer assemblages from the Goro lobe, due to similar frequencies of *A. parkinsoniana – A. tepida* (Table 5).

*4.2 Quantitative paleoecological data from the fossil record*

The distance between modern and core samples in terms of species composition was visualized through the wPCoA, which also allowed to estimate paleoecological changes in relation to environmental drivers in the modern North Adriatic ostracod and foraminifer biofacies (Figs.6-8).

In core 205S9, the trajectory of ostracod assemblages crosses the multivariate space of sites from biofacies O5-O4-O2, and then turns back (Fig. 6B). This reflects a decrease in paleobathymetry from transgressive to highstand assemblages (ca. 25–15 ± 1 m water depth), with a scattered higher water depth value at the delta front transition (ca. 21 ± 1 m), paralleled by a similar trend in sand concentration (from ca. 62 ± 3% to 26 ± 4%, up to >50% in the delta front transition; Fig. 6A; Table 6). The trajectory of transgressive benthic foraminifers from core 205S9 crosses the area of biofacies F3, F2 and F1, mirroring a progressive decrease in water depth (from ca. 19 ± 1 m to 11 ± 2 m) and a parallel increase in organic matter (ca. 0.8 ± 0.3–2.7 ± 0.6%).

The trajectory of fossil ostracod assemblages in core EM13 extends through the upper multivariate space, approximately parallel to the first axis of ordination, crossing biofacies O5-O4-O2-O1 (Fig. 7B). The reconstructed bathymetry and sand evenly decrease throughout the core, from transgressive (27 ± 1 m water depth, 75 ± 4 % sand) to highstand (13 ± 1 m water depth, 4 ± 4 % sand) deposits. Benthic foraminifers show a zig-zag trajectory distributed through biofacies F5-F3-F2-F1, reflecting an overall decrease in paleo-water depth

(ca. from 27 ± 1 m in TST to 11 ± 2 m in HST) and increase in organic matter (ca. from 0.6 ± 0.3% in TST to 2.5 ± 0.6% in HST), with localized oscillations throughout the succession (Fig. 7A).

The trajectory of ostracods from core 187S4 resembles that of core 205S9, with a back and forth trend that crosses sites from biofacies O5-O4 and comes back towards biofacies O5 (Fig. 8B). In terms of paleobathymetry, it reflects decrease in water depth from transgressive (ca. 24 ± 1 m) to highstand (ca. 11 ± 1 m) assemblages, with a few oscillations within the Goro lobe. Estimated sand concentration decreases from transgressive barrier (ca. 71 ± 4%) to lower prodelta (ca. 30 ± 4%) deposits and increases in the upper portion of the Goro lobe (>50%). The relatively short core trajectory of benthic foraminifers that crosses biofacies F3, F2 and F1 reflects higher paleobathymetry in TST (ca. 18 ± 1 m) and almost stable, lower water depths throughout highstand prodelta deposits (ca. 12 ± 1 m). Accordingly, organic matter increases from TST to HST, with relatively constant values across the Goro lobe (0.8 ± 0.3–2.6 ± 0.6%, Fig. 8A).

Differences between study cores and systems tracts can be visualized in a main effects plot (Fig. 9), where the centroids of each sediment unit are distributed in a multivariate space. Ostracod and foraminifer plots display the maximum distance on a systems tract-scale, with the centroids of transgressive assemblages being clearly separated from the highstand (delta lobe) ones. Concerning the study cores, centroids of 187S4 and 205S9 plot relatively close to each other showing negative PCoA axes scores for ostracods and positive values for foraminifers. Core EM13 is distinctly separated in both plots, with positive values of both axes in the ostracod plot and negative scores in the foraminifer PCoA.

## 5. Discussion

### *5.1 Know your setting: assessing the resolution of shallow-marine benthic ostracod and foraminifer records*

The high contrast between centroids of systems tract in the main effects plot indicates that both ostracods and foraminifers efficiently discriminate transgressive from highstand deltaic deposits (Fig. 9). Abundant opportunistic taxa in deltaic sediments (i.e., *L. ramosa, Palmoconcha turbida, Pontocythere turbida* and *A.*

*parkinsoniana – A. tepida*; Lachenal and Bodergat, 1988, 1990; Jorissen et al., 2018) drive the high dissimilarity with transgressive assemblages. Ostracods and foraminifers also highlight differences between cores, discriminating core EM13, which geographically lies between two delta lobes, from the markedly similar cores 187S4 and 205S9 located near paleo-river mouths (Figs. 1, 9). The unique character of core EM13 is ascribed to transgressive assemblages with abundant epiphytic foraminifers, i.e., *B. granulata*, *N. terquemi*, *R. bradyi* and *A. mamilla* (Langer, 1993; Sgarrella and Moncharmont Zei, 1993; Table 5), influencing the centroid position towards negative values of axis 1 (Fig. 7). Ostracods show marked dissimilarities in progradational deltaic deposits of core EM13, due to the dominance of the mud-lover *L. ramosa* (Barbieri et al., 2019) in the Goro lobe that determine a shift towards positive axis 1 values characteristic of highstand delta lobes. Core EM13 also shows the highest faunal turnover (Figs. 6B-8B), suggesting that paleoecological variations are better recorded at distal locations.

The comparison between modern and fossil assemblages with the AM technique allowed to obtain further insights in the paleoenvironmental record provided by each faunal group. In transgressive assemblages, the significant similarity with sites on the shallow North Adriatic relict sand barriers (biofacies O5, Figs. 2-5) is based on sand-related ostracods, such as *Semicytherura* spp. (including *S. incongruens*), *Pontocythere turbida, Loxoconcha* ex gr. *rhomboidea, S. napoliana* and *Cytheretta* spp. (Bonaduce et al., 1975; Frezza and Di Bella, 2015). Ostracods track the same deposit in the Po Delta subsurface and in the northern Adriatic shelf, as biofacies O5 is developed on sediment-starved sand ridges shaped from the reworking of relict transgressive sands (Trincardi et al., 1994; Correggiari et al., 1996). Therefore, reconstructed values of water depth reflect the geographic position of the deposit on the shelf instead of representing a true modern analog (Figs. 6A-8A). Concerning benthic foraminifers, the similarity to modern sites depleted in organic matter (biofacies F3, F5) is mostly driven by organic matter-sensitive taxa (*Triloculina* ex gr. *trigonula*, *Adelosina* spp., *Cycloforina* spp., *Siphonaperta aspera, B. granulata*, *N. terquemi*, *R. bradyi* and *A. mamilla*; Jorissen, 2018), widespread in the modern, shallow North Adriatic shelf (Barbieri et al., 2019).

In prograding delta lobes, the similarity with modern assemblages is driven by abundances of opportunistic taxa, particularly *Palmoconcha turbida, Pontocythere turbida, S. incongruens* and *A. parkinsoniana – A. tepida.* The presence of non-analog samples (Figs. 2-5) is ascribed to differences in assemblage composition or to under-representative modern dataset.

The paucity of significant modern analogs in the Volano lobe is determined by the marked compositional differences with modern assemblages. Ostracod and foraminifer taxa abundant in the Volano assemblages show contrasting ecological characteristics. Specifically, sand-related ostracods (*Pontocythere turbida, Loxoconcha* ex gr. *rhomboidea*, *S. napoliana*, *Semicytherura* spp.) are associated to taxa preferring fine-grained (*Palmoconcha turbida, S. versicolor*) or mixed (*Callistocythere* spp.) substrates (Bonaduce et al., 1975; Arbulla et al., 2004; Frezza and Di Bella, 2015). Similarly, benthic foraminifer assemblages from the lower Volano lobe of core EM13 include moderate frequencies of species tolerant (*A. parkinsoniana – A. tepida, A. perlucida, Cribroelphidium* ex gr. *granosum*) and sensitive (*Triloculina* ex gr. *trigonula*) to organic matter (Jorissen et al., 2018). Such microfossil assemblages chronologically overlap the development of wave-influenced cuspate and arcuate deltas characterized by a marked longshore transport component (Ciabatti, 1967; Amorosi et al., 2019). In wave-dominated deltas, fine-grained sediments supplied by rivers can be reworked, integrated within the delta or transported alongshore by wave-induced longshore currents. Even under high fluvial discharge regimes, waves can strongly affect delta dynamics in case of episodic high-energy events (Anthony, 2015). In the microtidal Mediterranean Sea, an example is represented by the Ombrone delta, where muddy sediments brought by episodic floods are transported alongshore by wave-induced currents on the long term (Tortora, 1999). As a result, benthic ostracod and foraminifer assemblages from the shallow Ombrone prodelta are composed of species with divergent ecological preferences (Frezza and Carboni, 2009; Frezza and Di Bella, 2015). Therefore, the absence of significant analogs in the Volano lobe still provides significant information, specifically, the absence of similar processes currently acting in the modern reference set. In fact, the high amount of riverine sediment and organic matter supplied by the lobate Po Delta represents the main forcing

on the meiofaunal zonation in the present-day North Adriatic system, whereas along-shore transport mostly operates in the southern Adriatic, where low fluvial inputs are recorded (Frignani et al., 2005; Barbieri et al., 2019).

A particular case is represented by the paucity of significant modern analogs for the Goro ostracod assemblages in core EM13, determined by the higher abundance of *L. ramosa* in fossil assemblages (ca. 70% vs. ca. 50% in modern communities). *Leptocythere ramosa* is one of the most opportunistic marine ostracods: abundant in transitional settings subject to mixed marine-freshwater contribution, it is strongly positively correlated with organic matter and prefers fine-grained bottoms at shallow depth (Uffenorde, 1972; Montenegro and Pugliese, 1996; Barbieri et al., 2019). To our knowledge, very high concentrations (>60%) are not reported from present-day environments. In sedimentary successions, *L. ramosa* is abundant at the transition from lagoonal to deltaic deposits or in proximal prodelta intervals (Carboni et al., 2002; Rossi, 2009). Studies on mollusks have shown that higher concentrations of opportunistic taxa in marine fossil assemblages are connected to rapid multiple invasions that are hardly preserved individually in the stratigraphic record (Levinton, 1970; Pearson and Rosenberg, 1978). Considering the paleoecological affinity of mollusks and ostracods (Amorosi et al., 2014; Rossi et al., 2018), we cannot rule out that *L. ramosa*-dominated assemblages in core EM13 were determined by comparable processes. In such nearshore river-influenced settings severely impacted by organic enrichments, the estimated paleoecological information is not necessarily incorrect as opportunistic population dynamics could greatly affect the dissimilarity with modern assemblages.

Finally, the lack of sites in the modern dataset could lead to biased assignments, as for the topmost prodelta ostracod assemblages of core 205S9. The similarity with a modern site on relict sands at ca. 30-40 m water depth (biofacies O6) is documented by the high abundance of *Pontocythere turbida*. However, this taxon is reported as dominant in the shallow prodelta, delta front, and shoreface zones of the Western Adriatic coast (Ruggieri, 1952; Colalongo, 1969), which were not sampled in the dataset used in the present work (>8 m water depth; (Breman, 1975).

### *5.2 Meiofauna-based paleoecological reconstructions: transgressive deposits*

Bathymetric estimates from transgressive benthic ostracods and foraminifers show some discrepancies (Figs.6A-8A). Based on analogies with modern Adriatic sites (see section 5.1), we consider more reliable the values provided by benthic foraminifers, which indicate an average water depth of ca. 18 ± 1 m at cores 187S4 and 205S9, and of 26 ± 1 m for EM13 (Table 6), in accordance with its distal position (Fig. 1). Significant modern analogs for transgressive ostracod assemblages indicate the onset of sediment-starved conditions in the whole study area during the last phases of transgression (ca. 8.5-7.0 cal kyr B.P.; Bruno et al., 2017), as also supported by low organic matter concentrations indicated by foraminifers (Figs. 6A-8A). Comparable foraminifer assemblages are reported from shallow-water, coarse-grained bottoms with low concentrations of refractory organic matter, such as relict deltaic deposits subject to high-energy conditions and sediment reworking (Goineau et al., 2015).

Paleoecological insights retrieved from transgressive microfossil assemblages are consistent with the early Holocene paleogeography, when a backstepping wave-dominated estuary occupied the modern Po coastal plain (Bruno et al., 2017). At the estuary mouth, transgressive barriers were affected by high-energy wave action and offshore deposits developed under a reduced sediment influx due to sediment trapping in the estuarine system (Bruno et al., 2017; Amorosi et al., 2019).

### *5.3 Meiofauna-based paleoecological reconstructions: highstand delta lobe deposits*

In prodelta successions, ostracods and benthic foraminifers provide similar water depth estimates, tracking a major decrease in paleobathymetry from bottom to top (Figs. 6A-8A). Overall, benthic foraminifers show more regular trends and suggest slightly shallower water depths than ostracods (13 ± 1 m and 15 ± 1 m on average, respectively), but these differences fall within the range of the standard error, with a few exceptions mostly connected to the lack of significant modern analogs (Figs. 2-4, 6-8). No significant paleobathymetric differences are recorded at proximal (core 205S9, 187S4) and distal (core EM13) locations. The different driving

factors that govern benthic ostracod and foraminifer distribution in the marine realm may account for local discrepancies in water depth and meiofaunal zonation (see section 5.1) (Yasuhara et al., 2012; Barbieri et al., 2019). Under highstand conditions, approaching river outlets due to delta progradation are consistent with a decrease in water depth, as observed in modern deltaic systems (Lavoie et al., 2014; Bomer et al., 2019), including the Po Delta (Correggiari et al., 2005b; Bosman et al., 2020). The relatively stable paleobathymetry recorded in ca. 10 m-thick upper prodelta deposits is ascribed to the rapid accumulation of riverine material that resulted in the deposition of expanded prodelta successions, with abundant opportunistic benthic ostracods and foraminifers that benefitted from continental organic matter inputs (Goineau et al., 2012; Frezza and Di Bella, 2015). High organic matter concentrations estimated from benthic foraminifers (2.1 ± 0.4 on average; Figs. 6A-8A) mostly linked to degraded, continental organic material are in accordance with data from the major deltaic systems of the Mediterranean (Goineau et al., 2011).

*5.3.1 Volano lobe*

Organic matter levels reconstructed from benthic foraminifers reflect the development of delta lobes. The good chronological resolution at core locations 205S9 and EM13 documents an increase in organic matter after the demise of the Roman Empire, when the countryside was abandoned and channel regulation ended, causing widespread inland flooding (Stefani and Vincenzi, 2005). Unstable river regime and high discharge are confirmed by relatively high organic matter concentrations (Figs. 4A, 5A), likely of continental origin that is typically associated to proximal prodelta settings with dominant *A. tepida – A. parkinsoniana* (Goineau et al., 2015). Nevertheless, abundant riverine organic inputs hardly reached updrift, distal locations at that time, as confirmed by the lower concentrations in core EM13 (1.5 ± 0.4 % vs. 2.1 ± 0.4 % in 205S9; Table 6).

High sand concentrations (Figs. 6-7A; Table 6) support considerable influence by longshore currents at both study sites, in accordance with the arcuate morphology of the Volano lobe (Fig. 1). In updrift position (EM13), a first phase of low sediment supply far from river outlets is suggested by analogy with ostracod assemblages on relict sands. After ca. 1.6-1.5 kyr B.P., ostracods track the approaching Volano lobe, with persistent longshore

currents and low to moderate sediment supply at shallow water depth (Figs. 3, 7). The increase of ostracod-derived sand concentration in the upper prodelta and within delta front transition deposits at proximal locations (core 205S9) is consistent with higher hydrodynamic conditions at the transition to the delta front in microtidal Mediterranean deltas (Lavoie et al., 2014; Ciampalini et al., 2015).

High sand concentration estimated from ostracods that highlight strong hydrodynamic conditions, along with increasing organic matter levels traced by benthic foraminifers, efficiently document the development of the Volano lobe. The cuspate morphology provides evidences for wave influence, nevertheless, abundant sediment supply from the Po River is recorded by sediment geochemistry and high sedimentation rates (Amorosi et al., 2020).

*5.3.2 Goro lobe*

Strong sediment and organic matter inputs of continental origin in proximity to a river mouth are consistent with benthic foraminifers throughout prodelta deposits, both at the proximal location of core 187S4 and at the distal EM13 site (Table 6, Figs. 7-8A).

In core 187S4, similarities with modern ostracod communities and high estimated sand concentrations suggest an important longshore drift component, whereas an abundance of fine-grained sediments and possible oxygen deficiency are recorded at the downdrift location (Figs. 3-4, 7-8).

The “Ficarolo avulsion” in the XII century AD caused a major switch from the Volano to Goro delta lobes. This event is recorded by localized low organic matter levels from benthic foraminifers, without significant associated paleobathymetric variations (Fig. 7A). The onset of the Goro lobe occurred at low water depth (<15 m), possibly due to decreasing accommodation after the progradation of the downdrift Volano lobe (Correggiari et al., 2005a). Afterwards, the increased fluvial discharge in response to the late Middle Ages climatic instability (including the Little Ice Age) and anthropogenic activity that led to the major Po delta lobe outbuilding (Veggiani, 1990; Stefani and Vincenzi, 2005) is documented as changes in sediment dynamics by

ostracods (biofacies O1), which suggest increased riverborne sediment supply. Structure and composition of ostracod communities suggest unstable environmental conditions in a mud-dominated, shallow-marine environment subject to enrichment in continental organic matter, in accordance with the accumulation of thick flood layers that promoted the rapid progradation of the Goro lobe (Correggiari et al., 2005b). At seaward locations, extremely high sediment and organic-matter supplies are recorded by mud-belt microfossil assemblages (Rossi and Vaiani, 2008; Rossi, 2009; Barbieri et al., 2017) responding to both refractory and labile organic matter of continental and marine origin, respectively (Diz et al., 2006; Mojtahid et al., 2009; Goineau et al., 2012).

## 6. Conclusions

Integrated analyses of benthic ostracods and foraminifers from the marine Holocene succession of the Po Delta provide the opportunity to assess the paleoecological information recorded by individual microfossil groups in past river-influenced shelves. The comparison with the modern North Adriatic reference set through multivariate analyses revealed to be a powerful tool for investigating meiofaunal dynamics in relation to coastal and deltaic evolution. Specifically, we reconstructed and connected three environmentally significant parameters (water depth, sand and organic matter concentrations) that allow to characterize delta dynamics in shallow-marine, river-influenced settings.

- We demonstrated that benthic ostracods and foraminifers discriminate transgressive from highstand units. Furthermore, microfossils allow to identify locations at different distance from paleo-river mouths. Particularly, lobe-fringe deposits seem to be more suitable for paleoecological studies, as the highest faunal turnover in response to major changes in delta regimes is recorded distally.

- We stress that an extensive knowledge of the modern reference set should drive a critical interpretation of (non-)analogies with fossil assemblages. Significant modern analogs could mirror non-true environmental conditions (e.g., estimated water depth from transgressive relict ostracod samples). On the

other hand, the lack of significant modern analogs can be important, as in our study reflects wave-influenced deltaic conditions not recorded in the modern dataset. However, other factors, such as population dynamics and limitations in the modern reference set may also influence the detected paleoecological information.

- We show the complementarity of marine benthic ostracods and foraminifers as proxies for high-resolution paleoecological reconstructions in river-influenced successions. Ostracods provide insights into depositional regimes, furnishing an overview of bottom-water conditions in terms of sediment supply, hydrodynamic energy and, locally, oxygen conditions. Transgressive ostracod assemblages indicate sediment starvation, whereas highstand ostracods reflect position of the study site in relationship with the river mouth in the three-dimensional space (along-dip and along-strike) and delta regimes. Benthic foraminifers discriminate localized transgressive paleoenvironmental conditions and provide information about highstand changes in riverine input in terms of organic matter, in relationship with the position from river mouths.

## Acknowledgements

The authors acknowledge Regione Emilia Romagna – RER for providing access to core material. We thank Bruno Campo for the support with radiocarbon dates calibration. Two anonymous reviewer and the handling editor are kindly acknowledged for the constructive suggestions.

## References


Amorosi, A., Colalongo, M.L., 2005. The linkage between alluvial and coeval nearshore marine successions: evidence from the late Quaternary record of the Po River Plain, Italy. Spec. Publs int. Ass. Sediment. 35, 257–275.

Amorosi, A., Centineo, M.C., Colalongo, M.L., Pasini, G., Sarti, G., Vaiani, S.C., 2003. Facies Architecture and Latest Pleistocene–Holocene Depositional History of the Po Delta (Comacchio Area), Italy. The Journal of Geology 111, 39–56. https://doi.org/10.1086/344577

Amorosi, A., Dinelli, E., Rossi, V., Vaiani, S.C., Sacchetto, M., 2008. Late Quaternary palaeoenvironmental evolution of the Adriatic coastal plain and the onset of Po River Delta. Palaeogeography, Palaeoclimatology, Palaeoecology 268, 80–90. https://doi.org/10.1016/j.palaeo.2008.07.009

Amorosi, A., Rossi, V., Scarponi, D., Vaiani, S.C., Ghosh, A., 2014. Biosedimentary record of postglacial coastal dynamics: high-resolution sequence stratigraphy from the northern Tuscan coast (Italy): Postglacial coastal dynamics, N Tuscan coast, Italy. Boreas 43, 939–954. https://doi.org/10.1111/bor.12077

Amorosi, A., Bruno, L., Campo, B., Morelli, A., Rossi, V., Scarponi, D., Hong, W., Bohacs, K.M., Drexler, T.M., 2017. Global sea-level control on local parasequence architecture from the Holocene record of the Po Plain, Italy. Marine and Petroleum Geology 87, 99–111. https://doi.org/10.1016/j.marpetgeo.2017.01.020

Amorosi, A., Barbieri, G., Bruno, L., Campo, B., Drexler, T.M., Hong, W., Rossi, V., Sammartino, I., Scarponi, D., Vaiani, S.C., Bohacs, K.M., 2019. Three-fold nature of coastal progradation during the Holocene eustatic highstand, Po Plain, Italy – close correspondence of stratal character with distribution patterns. Sedimentology 66, 3029–3052. https://doi.org/10.1111/sed.12621

Amorosi, A., Bruno, L., Campo, B., Costagli, B., Dinelli, E., Hong, W., Sammartino, I., Vaiani, S.C., 2020. Tracing clinothem geometry and sediment pathways in the prograding Holocene Po Delta system through integrated core stratigraphy. Basin Res 32, 206–215. https://doi.org/10.1111/bre.12360

533 Anderson, P.M., Bartlein, P.J., Brubaker, L.B., Gajewski, K., Ritchie, J.C., 1989. Modern Analogues of Late-
534 Quaternary Pollen Spectra from the Western Interior of North America. Journal of Biogeography 16, 573.
535 https://doi.org/10.2307/2845212
536 Angue Minto'o, C.M., Bassetti, M.-A., Toucanne, S., Jouet, G., 2016. Distribution of ostracod and benthic
537 foraminiferal assemblages during the last 550kyr in the East-Corsica basin, western Mediterranean Sea: A
538 paleo-environmental reconstruction. Revue de Micropaléontologie 59, 83–96.
539 https://doi.org/10.1016/j.revmic.2016.01.002
540 Anthony, E.J., 2015. Wave influence in the construction, shaping and destruction of river deltas: A review.
541 Marine Geology 361, 53–78. https://doi.org/10.1016/j.margeo.2014.12.004
542 Arbulla, D., Pugliese, N., Russo, A., 2004. Ostracods from the National Park of La Maddalena Archipelago
543 (Sardinia, Italy). Bollettino della Società Paleontologica Italiana 43, 91–99.
544 Athersuch, J., Horne, D.J., Whittaker, J.E., 1989. Marine and brackish water ostracods, Synopses of the British
545 Fauna (New Series). Brill E.J., Leiden (345 pp).
546 Azzarone, M., Barbieri, G., Rossi, V., Gamberi, F., Trincardi, F., Scarponi, D., 2020. Linking benthic fauna and
547 seismic facies to improve stratigraphic reconstructions: the case of the Mid-Adriatic Deep since the late
548 glacial period (Central Adriatic Sea). Bollettino della Società Paleontologica Italiana 59, 9–23.
549 https://doi.org/10.4435/BSPI.2020.03
550 Barbieri, G., Amorosi, A., Vaiani, S.C., 2017. Benthic foraminifera as a key to delta evolution: A case study from
551 the late Holocene succession of the Po River Delta. Micropaleontology 63, 27–41.
552 Barbieri, G., Rossi, V., Vaiani, S.C., Horton, B.P., 2019. Benthic ostracoda and foraminifera from the North
553 Adriatic Sea (Italy, Mediterranean Sea): A proxy for the depositional characterisation of river-influenced
554 shelves. Marine Micropaleontology 153, 101772. https://doi.org/10.1016/j.marmicro.2019.101772
555 Bassetti, M.-A., Carbonel, P., Sierro, F.J., Perez-Folgado, M., Jouët, G., Berné, S., 2010. Response of ostracods to
556 abrupt climate changes in the Western Mediterranean (Gulf of Lions) during the last 30kyr. Marine
557 Micropaleontology 77, 1–14. https://doi.org/10.1016/j.marmicro.2010.06.004

558 Benito, X., Trobajo, R., Cearreta, A., Ibáñez, C., 2016. Benthic foraminifera as indicators of habitat in a
559 Mediterranean delta: implications for ecological and palaeoenvironmental studies. Estuarine, Coastal and
560 Shelf Science 180, 97–113. https://doi.org/10.1016/j.ecss.2016.06.001
561 Bomer, E.J., Bentley, S.J., Hughes, J.E.T., Wilson, C.A., Crawford, F., Xu, K., 2019. Deltaic morphodynamics and
562 stratigraphic evolution of Middle Barataria Bay and Middle Breton Sound regions, Louisiana, USA:
563 Implications for river-sediment diversions. Estuarine, Coastal and Shelf Science 224, 20–33.
564 https://doi.org/10.1016/j.ecss.2019.03.017
565 Bonaduce, G., Ciampo, G., Masoli, M., 1975. Distribution of Ostracoda in the Adriatic Sea, Pubblicazioni della
566 Stazione Zoologica di Napoli. Olschki L. S., Napoli, Italy (154 pp).
567 Bosman, A., Romagnoli, C., Madricardo, F., Correggiari, A., Remia, A., Zubalich, R., Fogarin, S., Kruss, A.,
568 Trincardi, F., 2020. Short-term evolution of Po della Pila delta lobe from time lapse high-resolution
569 multibeam bathymetry (2013–2016). Estuarine, Coastal and Shelf Science 233, 106533.
570 https://doi.org/10.1016/j.ecss.2019.106533
571 Breman, E., 1975. The distribution of Ostracodes in the bottom sediments of the Adriatic Sea (Ph.D. Thesis).
572 Free University of Amsterdam, the Netherlands (165 pp).
573 Bronk Ramsey, C., 2009. Bayesian Analysis of Radiocarbon Dates. Radiocarbon 51, 337–360.
574 https://doi.org/10.1017/S0033822200033865
575 Bruno, L., Bohacs, K.M., Campo, B., Drexler, T.M., Rossi, V., Sammartino, I., Scarponi, D., Hong, W., Amorosi, A.,
576 2017. Early Holocene transgressive palaeogeography in the Po coastal plain (northern Italy). Sedimentology
577 64, 1792–1816. https://doi.org/10.1111/sed.12374
578 Cacciari, M., Amorosi, A., Campo, B., Marchesini, M., Rossi, V., 2019. Palynology of the late Quaternary
579 succession of the Arno Plain (northern Italy): new insights on palaeoenvironmental trends and climate
580 dynamics. Bollettino della Società Paleontologica Italiana 201–221. https://doi.org/10.4435/BSPI.2019.16

581 Campo, B., Amorosi, A., Vaiani, S.C., 2017. Sequence stratigraphy and late Quaternary paleoenvironmental
582 evolution of the Northern Adriatic coastal plain (Italy). Palaeogeography, Palaeoclimatology, Palaeoecology
583 466, 265–278. https://doi.org/10.1016/j.palaeo.2016.11.016
584 Carboni, M.G., Bergamin, L., Di Bella, L., Iamundo, F., Pugliese, N., 2002. Palaeoecological evidences from
585 foraminifers and ostracods on Late Quaternary sea-level changes in the Ombrone river plain (central
586 Tyrrhenian coast, Italy). Geobios 35, 40–50. https://doi.org/10.1016/S0016-6995(02)00047-5
587 Ciabatti, M., 1967. Ricerche sull'evoluzione del Delta Padano. Giornale di Geologia 34, 381–406.
588 Ciampalini, A., Consoloni, I., Salvatici, T., Di Traglia, F., Fidolini, F., Sarti, G., Moretti, S., 2015. Characterization of
589 coastal environment by means of hyper- and multispectral techniques. Applied Geography 57, 120–132.
590 https://doi.org/10.1016/j.apgeog.2014.12.024
591 Clarke, K.R., 1993. Non-parametric multivariate analyses of changes in community structure. Austral. Ecol. 18,
592 117–143. https://doi.org/10.1111/j.1442-9993.1993.tb00438.x
593 Colalongo, M.L., 1969. Ricerche sugli Ostracodi nei fondali antistanti il delta del Po. Giornale di Geologia 36,
594 335–362.
595 Correggiari, A., Cattaneo, A., Trincardi, F., 2005a. Depositional Patterns in the Late Holocene Po Delta System,
596 in: Giosan, L., Bhattacharya, J.P. (Eds.), River Deltas–Concepts, Models, and Examples. SEPM Society for
597 Sedimentary Geology, pp. 365–392. https://doi.org/10.2110/pec.05.83.0365
598 Correggiari, A., Cattaneo, A., Trincardi, F., 2005b. The modern Po Delta system: Lobe switching and asymmetric
599 prodelta growth. Marine Geology 222–223, 49–74. https://doi.org/10.1016/j.margeo.2005.06.039
600 Correggiari, A., Roveri, M., Trincardi, F., 1996. Late Pleistocene and Holocene evolution of the North Adriatic
601 Sea. Il Quaternario - Italian Journal of Quaternary Sciences 9, 697–704.
602 Cronin, T.M., DeMartino, D.M., Dwyer, G.S., Rodriguez-Lazaro, J., 1999. Deep-sea ostracode species diversity:
603 response to late Quaternary climate change. Marine Micropaleontology 37, 231–249.
604 https://doi.org/10.1016/S0377-8398(99)00026-2

605 Dasgupta, U., Barbieri, G., Vaiani, S.C., Ghosh, A., 2020. Potential and limits of benthic foraminiferal ecological
606 indices in paleoenvironmental reconstructions: a case from a Holocene succession of the Po Delta, Italy 66,
607 103–126.
608 Diz, P., Francés, G., Rosón, G., 2006. Effects of contrasting upwelling–downwelling on benthic foraminiferal
609 distribution in the Ría de Vigo (NW Spain). Journal of Marine Systems 60, 1–18.
610 https://doi.org/10.1016/j.jmarsys.2005.11.001
611 Faasse, M., 2013. The North American ostracod Eusarsiella zostericola (Cushman, 1906) arrives in mainland
612 Europe. BioInvasions Records 2, 1–4.
613 Fanget, A.-S., Bassetti, M.-A., Arnaud, M., Chiffoleau, J.-F., Cossa, D., Goineau, A., Fontanier, C., Buscail, R.,
614 Jouet, G., Maillet, G.M., Negri, A., Dennielou, B., Berné, S., 2013. Historical evolution and extreme climate
615 events during the last 400years on the Rhone prodelta (NW Mediterranean). Marine Geology 346, 375–391.
616 https://doi.org/10.1016/j.margeo.2012.02.007
617 Fanget, A.-S., Bassetti, M.-A., Fontanier, C., Tudryn, A., Berné, S., 2016. Sedimentary archives of climate and
618 sea-level changes during the Holocene in the Rhône prodelta (NW Mediterranean Sea). Clim. Past 12, 2161–
619 2179. https://doi.org/10.5194/cp-12-2161-2016
620 Flaux, C., Claude, C., Marriner, N., Morhangem C., 2013. A 7500-year strontium isotope record from the
621 northwestern Nile delta (Maryut lagoon, Egypt). Quaternary Science Reviews 78, 22–33.
622 Frezza, V., Carboni, M.G., 2009. Distribution of recent foraminiferal assemblages near the Ombrone River
623 mouth (Northern Tyrrhenian Sea, Italy). Revue de Micropaléontologie 52, 43–66.
624 https://doi.org/10.1016/j.revmic.2007.08.007
625 Frezza, V., Di Bella, L., 2015. Distribution of recent ostracods near the Ombrone River mouth (Northern
626 Tyrrhenian Sea, Italy). Micropaleontology 61, 101–114.
627 Frignani, M., Langone, L., Ravaioli, M., Sorgente, D., Alvisi, F., Albertazzi, S., 2005. Fine-sediment mass balance
628 in the western Adriatic continental shelf over a century time scale. Marine Geology 222–223, 113–133.
629 https://doi.org/10.1016/j.margeo.2005.06.016

630 Giacomelli, S., Rossi, V., Amorosi, A., Bruno, L., Campo, B., Ciampalini, A., Civa, A., Hong, W., Sgavetti, M., de
631 Souza Filho, C.R., 2018. A mid-late Holocene tidally-influenced drainage system revealed by integrated
632 remote sensing, sedimentological and stratigraphic data. Geomorphology 318, 421–436.
633 https://doi.org/10.1016/j.geomorph.2018.07.004
634 Goineau, A., Fontanier, C., Jorissen, F.J., Lansard, B., Buscail, R., Mouret, A., Kerhervé, P., Zaragosi, S., Ernoult,
635 E., Artéro, C., Anschutz, P., Metzger, E., Rabouille, C., 2011. Live (stained) benthic foraminifera from the
636 Rhône prodelta (Gulf of Lion, NW Mediterranean): Environmental controls on a river-dominated shelf.
637 Journal of Sea Research 65, 58–75. https://doi.org/10.1016/j.seares.2010.07.007
638 Goineau, A., Fontanier, C., Jorissen, F., Buscail, R., Kerhervé, P., Cathalot, C., Pruski, A.M., Lantoine, F.,
639 Bourgeois, S., Metzger, E., Legrand, E., Rabouille, C., 2012. Temporal variability of live (stained) benthic
640 foraminiferal faunas in a river-dominated shelf – Faunal response to rapid changes of the river influence
641 (Rhône prodelta, NW Mediterranean). Biogeosciences 9, 1367–1388. https://doi.org/10.5194/bg-9-1367-
642 2012
643 Goineau, A., Fontanier, C., Mojtahid, M., Fanget, A.-S., Bassetti, M.-A., Berné, S., Jorissen, F., 2015. Live–dead
644 comparison of benthic foraminiferal faunas from the Rhône prodelta (Gulf of Lions, NW Mediterranean):
645 Development of a proxy for palaeoenvironmental reconstructions. Marine Micropaleontology 119, 17–33.
646 https://doi.org/10.1016/j.marmicro.2015.07.002
647 Gooday, A.J., 2001. Benthic foraminifera, in: Steele, J.H., Thorpe, S.A., Turekian, K.K. (Eds.), Encyclopedia of
648 Ocean Sciences. Elsevier, pp. 336–347.
649 Goring, S., Pellatt, M.G., Lacourse, T., Walker, I.R., Mathewes, R.W., 2009. A new methodology for
650 reconstructing climate and vegetation from modern pollen assemblages: an example from British Columbia.
651 Journal of Biogeography 36, 626–638. https://doi.org/10.1111/j.1365-2699.2008.02021.x
652 Hammer, Ø., Harper, D.A.T., Ryan, P.D., 2001. PAST: paleontological statistics software package for education
653 and data analysis. Palaeontologia Electronica 4, 1–9.

654 Hohenegger, J., 2018. Foraminiferal growth and test development. Earth-Science Reviews 185, 140–162.
655 https://doi.org/10.1016/j.earscirev.2018.06.001
656 Horne, D.J., Holmes, J., Rodriguez-Lazaro, J., Viehberg, F.A., 2012. Ostracoda as Proxies for Quaternary Climate
657 Change, Developments in Quaternary Science. Elsevier.
658 Jackson, S.T., Williams, J.W., 2004. Modern analogs in quaternary paleoecology: here today, gone yesterday,
659 gone tomorrow? Annu. Rev. Earth Planet. Sci. 32, 495–537.
660 https://doi.org/10.1146/annurev.earth.32.101802.120435
661 Jorissen, F.J., 1988. Benthic foraminifera from the Adriatic Sea; principles of phenotypic variation, Utrecht
662 Micropaleontological Bulletins 37 (176 pp).
663 Jorissen, F., Nardelli, M.P., Almogi-Labin, A., Barras, C., Bergamin, L., Bicchi, E., El Kateb, A., Ferraro, L., McGann,
664 M., Morigi, C., Romano, E., Sabbatini, A., Schweizer, M., Spezzaferri, S., 2018. Developing Foram-AMBI for
665 biomonitoring in the Mediterranean: Species assignments to ecological categories. Marine
666 Micropaleontology 140, 33–45. https://doi.org/10.1016/j.marmicro.2017.12.006
667 Lachenal, A.M., Bodergat, A.M., 1988. Les ostracodes et l'évolution paléogéographique au Quaternaire récent
668 du site d'Ashtart (Golfe de Gabès, Tunisie Orientale). Geobios 21, 73–80.
669 Lachenal, A.M., Bodergat, A.M., 1990. Les ostracodes et les variations paléoeustatiques du Golfe de Gabès
670 (Méditerranée) depuis 30000 ans. Bulletin de la Société Géologique de France 8, 113–122.
671 Langer, M.R., 1993. Epiphytic foraminifera. Marine Micropaleontology 20, 235–265.
672 https://doi.org/10.1016/0377-8398(93)90035-V
673 Langone, L., Asioli, A., Correggiari, A., Trincardi, F., 1996. Age-depth modelling through the late Quaternary
674 deposits of the central Adriatic basin. Mem. Ist. Ital. Idrobiol. 55, 177–196.
675 Lavoie, C., Jiménez, J.A., Canals, M., Lastras, G., De Mol, B., Amblas, D., Liquete, C., De Batist, M., Hughes
676 Clarke, J.E., 2014. Influence on present-day coastal dynamics and evolution of a relict subaqueous delta
677 lobe: Sol de Riu lobe, Ebro Delta. Continental Shelf Research 74, 94–104.
678 https://doi.org/10.1016/j.csr.2013.11.021

679 Legendre, P., Gallagher, E.D., 2001. Ecologically meaningful transformations for ordination of species data.
680 Oecologia 129, 271–280. https://doi.org/10.1007/s004420100716
681 Legendre, P., De Cáceres, M., 2013. Beta diversity as the variance of community data: dissimilarity coefficients
682 and partitioning. Ecol. Lett. 16, 951–963. https://doi.org/10.1111/ele.12141
683 Levinton, J.S., 1970. The paleoecological significance of oppurtunistic species. Lethaia 3, 69–78.
684 https://doi.org/10.1111/j.1502-3931.1970.tb01264.x
685 Mendes, I., Gonzalez, R., Dias, J.M.A., Lobo, F., Martins, V., 2004. Factors influencing recent benthic
686 foraminifera distribution on the Guadiana shelf (Southwestern Iberia). Marine Micropaleontology 51, 171–
687 192. https://doi.org/10.1016/j.marmicro.2003.11.001
688 Mesquita-Joanes, F., Smith, A.J., Viehberg, F.A., 2012. The Ecology of Ostracoda Across Levels of Biological
689 Organisation from Individual to Ecosystem: A Review of Recent Developments and Future Potential, in:
690 Horne, D.J., Holmes, J.A., Rodriguez-Lazaro, J., Viehberg, F.A. (Eds.), Ostracoda as Proxies for Quaternary
691 Climate Change. Elsevier, pp. 15–35. https://doi.org/10.1016/B978-0-444-53636-5.00002-0
692 Mojtahid, M., Jorissen, F., Lansard, B., Fontanier, C., Bombled, B., Rabouille, C., 2009. Spatial distribution of live
693 benthic foraminifera in the Rhône prodelta: Faunal response to a continental–marine organic matter
694 gradient. Marine Micropaleontology 70, 177–200. https://doi.org/10.1016/j.marmicro.2008.12.006
695 Montenegro, M.E., Pugliese, N., 1996. Autecological remarks on the ostracod distribution in the Marano and
696 Grado Lagoons (Northern Adriatic Sea, Italy). Bollettino della Società Paleontologica Italiana Spec. Vol. 3,
697 123–132.
698 Murray, J.W., 2001. The niche of benthic foraminifera, critical thresholds and proxies. Marine
699 Micropaleontology 41, 1–7. https://doi.org/10.1016/S0377-8398(00)00057-8
700 Murray, J.W., 2006. Ecology and Applications of Benthic Foraminifera. Cambridge University Press, Cambridge
701 (426 pp).

Oksanen, J., Blanchet, G., Friendly, M., Kindt, R., Legendre, P., McGlinn, D., Minchin, P.R., O'Hara, R.B., Simpson, G.L., Solymos, P., Stevens, M.Henry.H., Szoecs, E., Wagner, H., 2019. Vegan: Community Ecology Package. R package version 2.5-6. https://CRAN.R-project.org/package=vegan

Overpeck, J.T., Webb, T., Prentice, I.C., 1985. Quantitative Interpretation of Fossil Pollen Spectra: Dissimilarity Coefficients and the Method of Modern Analogs. Quat. Res. 23, 87–108. https://doi.org/10.1016/0033-5894(85)90074-2

Pascual, A., Rodriguez-Lazaro, J., Martín-Rubio, M., Jouanneau, J.-M., Weber, O., 2008. A survey of the benthic microfauna (foraminifera, Ostracoda) on the Basque shelf, southern Bay of Biscay. Journal of Marine Systems 72, 35–63.

Pearson, T.H., Rosenberg, R., 1978. Macrobenthic succession in relation to organic enrichment and pollution of the marine environment. Oceanogr. Mar. Biol. Ann. Rev. 16, 229–311.

Reimer, P.J., Bard, E., Bayliss, A., Beck, J.W., Blackwell, P.G., Ramsey, C.B., Buck, C.E., Cheng, H., Edwards, R.L., Friedrich, M., Grootes, P.M., Guilderson, T.P., Haflidason, H., Hajdas, I., Hatté, C., Heaton, T.J., Hoffmann, D.L., Hogg, A.G., Hughen, K.A., Kaiser, K.F., Kromer, B., Manning, S.W., Niu, M., Reimer, R.W., Richards, D.A., Scott, E.M., Southon, J.R., Staff, R.A., Turney, C.S.M., van der Plicht, J., 2013. IntCal13 and Marine13 Radiocarbon Age Calibration Curves 0–50,000 Years cal BP. Radiocarbon 55, 1869–1887. https://doi.org/10.2458/azu_js_rc.55.16947

Rodriguez-Lazaro, J., Ruiz-Muñoz, F., 2012. A General Introduction to Ostracods: Morphology, Distribution, Fossil Record and Applications, in: Horne, D.J., Holmes, J.A., Rodriguez-Lazaro, J., Viehberg, F.A. (Eds.), Ostracoda as Proxies for Quaternary Climate Change. Developments in Quaternary Sciences 17. Elsevier, pp. 1–14. https://doi.org/10.1016/B978-0-444-53636-5.00001-9

Rossi, V., 2009. Ostracod assemblages from Holocene subsurface deposits of modern Po Delta: a palaeoenvironmental proxy record. Bollettino della Società Paleontologica Italiana 48, 95–103.

Rossi, V., Vaiani, S.C., 2008. Benthic foraminiferal evidence of sediment supply changes and fluvial drainage reorganization in Holocene deposits of the Po Delta, Italy. Marine Micropaleontology 69, 106–118. https://doi.org/10.1016/j.marmicro.2008.07.001

Rossi, V., Azzarone, M., Capraro, L., Faranda, C., Ferretti, P., Macrì, P., Scarponi, D., 2018. Dynamics of benthic marine communities across the Early-Middle Pleistocene boundary in the Mediterranean region (Valle di Manche, Southern Italy): Biotic and stratigraphic implications. Palaeogeography, Palaeoclimatology, Palaeoecology 495, 127–138. https://doi.org/10.1016/j.palaeo.2017.12.042

Ruggieri, G., 1952. Nota preliminare sugli Ostracodi di alcune spiagge adriatiche. Note del Laboratorio di Biologia Marina di Fano 1, 57–64.

Salvi, G., Buosi, C., Arbulla, D., Cherchi, A., De Giudici, G., Ibba, A., De Muro, S., 2015. Ostracoda and foraminifera response to a contaminated environment: the case of the Ex-Military Arsenal of the La Maddalena Harbour (Sardinia, Italy). Micropaleontology 61, 115–133.

Scarponi, D., Azzarone, M., Kusnerik, K., Amorosi, A., Bohacs, K.M., Drexler, T.M., Kowalewski, M., 2017. Systematic vertical and lateral changes in quality and time resolution of the macrofossil record: Insights from Holocene transgressive deposits, Po coastal plain, Italy. Marine and Petroleum Geology 87, 128–136. https://doi.org/10.1016/j.marpetgeo.2017.03.031

Schellenberg, S.A., 2007. Marine Ostracods, in: Elias, S.A. (Ed.), Encyclopedia of Quaternary Science. Elsevier, pp. 2046–2062.

Sciuto, F., Rosso, A., Sanfilippo, R., 2015. Ostracods from mid-outer shelf bottoms of the Ciclopi Islands Marine Protected Area (Ionian Sea, Eastern Sicily). Bollettino della Società Paleontologica Italiana 54, 131–145. https://doi.org/10.4435/BSPI.2015.09

Sgarrella, F., Moncharmont Zei, M., 1993. Benthic Foraminifera of the Gulf of Naples (Italy): systematics and autoecology. Bollettino della Società Paleontologica Italiana 32, 145–264.

Simpson, G.L., 2007. Analogue Methods in Palaeoecology: Using the analogue Package. Journal of Statistical Software 22, 1–29.

Simpson, G.L., Oksanen, J., 2020. analogue: Analogue and weighted averaging methods for palaeoecology. https://cran.r-project.org/package=analogue

Stefani, M., Vincenzi, S., 2005. The interplay of eustasy, climate and human activity in the late Quaternary depositional evolution and sedimentary architecture of the Po Delta system. Marine Geology 222–223, 19–48. https://doi.org/10.1016/j.margeo.2005.06.029

Sutherland, K.R., Dabiri, J.O., Koehl, M.A.R., 2011. Simultaneous field measurements of ostracod swimming behavior and background flow: Ostracod swimming behavior in flow. Limnol. Oceanogr. 1, 135–146. https://doi.org/10.1215/21573698-1472410

Tanaka, H., Yasuhara, M., Carlton, T., 2018. Transoceanic transport of living marine Ostracoda (Crustacea) on tsunami debris from the 2011 Great East Japan Earthquake. Aquatic Invasions 13, 125–135. https://doi.org/10.3391/ai.2018.13.1.10

Tortora, P., 1999. Sediment distribution on the Ombrone River Delta seafloor and related dispersal processes. Geologica Romana 35, 211–218.

Triantaphyllou, M.V., Tsourou, T., Koukousioura, O., Dermitzakis, M.D., 2005. Foraminiferal and ostracod ecological patterns in coastal environments of SE Andros Island (Middle Aegean Sea, Greece). Revue de Micropaléontologie 48, 279–302. https://doi.org/10.1016/j.revmic.2005.09.003

Trincardi, F., Correggiari, A., Roveri, M., 1994. Late Quaternary transgressive erosion and deposition in a modern epicontinental shelf: The Adriatic semienclosed basin. Geo-Marine Letters 14, 41–51. https://doi.org/10.1007/BF01204470

Uffenorde, H., 1972. Ökologie und jahreszeitliche Verteilung rezenter benthonischer Ostracoden des Limski kanal bei Rovinj (nördliche Adria). Göttinger Arb. Geol. Paläont. 13 (142 pp).

Vacchi, M., Marriner, N., Morhange, C., Spada, G., Fontana, A., Rovere, A., 2016. Multiproxy assessment of Holocene relative sea-level changes in the western Mediterranean: Sea-level variability and improvements in the definition of the isostatic signal. Earth-Science Reviews 155, 172–197. https://doi.org/10.1016/j.earscirev.2016.02.002

Veggiani, A., 1990. Fluttuazioni climatiche e trasformazioni ambientali nel territorio imolese dall'alto medioevo all'età moderna, in: Mancini, F., Gioberti, M., Veggiani, A. (Eds.), Imola Nel Medioevo. Imola, pp. 41–102.

Weinmann, A.E., Goldstein, S.T., 2017. Landward-directed dispersal of benthic foraminiferal propagules at two shallow-water sites in the Doboy Sound area (Georgia, U.S.A.). Journal of Foraminiferal Research 47, 325–336. https://doi.org/10.2113/gsjfr.47.4.325

Wickham, H., 2016. ggplot2: Elegant Graphics for Data Analysis. Springer-Verlag New York. http://ggplot2.org

Wood, S.N., 2011. Fast stable restricted maximum likelihood and marginal likelihood estimation of semiparametric generalized linear models. Journal of the Royal Statistical Society (B) 73, 3–36.

Yasuhara, M., Hunt, G., Cronin, T.M., Hokanishi, N., Kawahata, H., Tsujimoto, A., Ishitake, M., 2012. Climatic forcing of Quaternary deep-sea benthic communities in the North Pacific Ocean. Paleobiology 38, 162–179. https://doi.org/10.1666/10068.1

Yasuhara, M., Tittensor, D.P., Hillebrand, H., Worm, B., 2017. Combining marine macroecology and palaeoecology in understanding biodiversity: microfossils as a model: Marine macroecology-palaeoecology integration. Biol. Rev. 92, 199–215. https://doi.org/10.1111/brv.12223

790 **Tables**

| Core | Sample depth (m) | Dated material | Conventional 14C age (yr B.P.) | Calibrated age 2σ range (yr B.P.) | Calibrated age mean (yr B.P.) | σ | Laboratory | References |
|---|---|---|---|---|---|---|---|---|
| 187 S4 | 25.45 | Peat | 8020 ± 70 | 9035-8635 | 8875 | 115 | Beta analytic (FL, USA) | Sheet 187, Geological Map of Italy at 1:50,000 scale |
| 187 S4 | 20.70 | Shell fragments | 1590 ± 24 | 1310-1185 | 1270 | 25 | KIGAM (Korea) | This study |
| EM13 | 10.90 | Shell | 840 ± 40 | 650–510 | 580 | 40 | KIGAM (Korea) | Amorosi et al., 2017 |
| EM13 | 17.50 | Wood | 1060 ± 30 | 1055–925 | 975 | 35 | KIGAM (Korea) | Amorosi et al., 2017 |
| EM13 | 22.65 | Shell | 1900 ± 40 | 1700–1420 | 1570 | 50 | KIGAM (Korea) | Amorosi et al., 2017 |
| EM13 | 26.75 | Wood | 8040 ±50 | 9090–8715 | 8900 | 100 | KIGAM (Korea) | Amorosi et al., 2017 |
| EM13 | 29.00 | Peat | 8500 ± 50 | 9545–9440 | 9500 | 30 | KIGAM (Korea) | Amorosi et al., 2017 |
| EM13 | 32.00 | Wood | 9080 ± 50 | 10385–10175 | 10250 | 50 | KIGAM (Korea) | Amorosi et al., 2017 |
| 205 S9 | 8.40 | Organic clay | 2013 ± 57 | 1560–1285 | 1425 | 70 | ENEA (Italy) | Amorosi et al., 2003 |
| 205 S9 | 22.40 | Shell | 2000 ± 40 | 1800–1570 | 1680 | 60 | KIGAM (Korea) | Campo et al., 2017 |
| 205 S9 | 25.30 | Shell | 6440 ± 50 | 7225–6950 | 7080 | 70 | KIGAM (Korea) | Campo et al., 2017 |
| 205 S9 | 26.95 | Shells / Lentidium | 7975 ± 30 | 8382–8192 | 8298 | 50 | Keck-CCAMS (CA., USA) | Scarponi et al., 2013 |
| 205 S9 | 26.95 | Shells / Varicorbula | 8075 ± 30 | 8501–8316 | 8398 | 45 | Keck-CCAMS (CA., USA) | Scarponi et al., 2013 |
| 205 S9 | 31.20 | Plant fragments | 9500 ± 80 | 11,110–10,570 | 10,840 | 160 | ETH (Switzerland) | Amorosi et al., 2003 |
| 205 S9 | 35.30 | Wood | 18,830 ± 140 | 23,035–22,410 | 22,710 | 165 | ETH (Switzerland) | Amorosi et al., 2003 |

791

792 **Table 1** – List of radiometric ages.

793

| Benthic group | Modern biofacies | Color | Key taxa | Abiotic parameters' mean values | | | | Geographic distribution | Environmental features |
|---|---|---|---|---|---|---|---|---|---|
| | | | | Depth (m) | Sand (%) | Organic matter (%) | $CaCO_3$ (%) | | |
| Ostracods | O1 | | *Palmoconcha turbida, L. ramosa*, other *Leptocythere* | 11.7 | 6.3 | 3.9 | 21.8 | A few km south of the Po Delta | High sediment and organic matter supply determining recurrent oxygen deficiency at shallow depth |
| | O2 | | *S. incongruens, Palmoconcha turbida* | 17.0 | 4.9 | 1.1 | 32.1 | Adige river mouth; South of the Po Delta | Moderate sediment supply at intermediate water depth |
| | O3 | | *C. neapolitana, L. ramosa, S. versicolor* | 27.5 | 2.2 | 1.4 | 28.1 | Mud belt | High sediment and organic matter supply south of the feeding mouths at moderate water depth |
| | O4 | | *S. incongruens, Pontocythere turbida, Palmoconcha turbida, Xestoleberis spp.* | 12.3 | 51.9 | 0.5 | 50.4 | Along the coast, North and South of the Po Delta | Low to moderate sediment supply, sandy substrates with high $CaCO_3$ subject to strong longshore currents at shallow depth, outside of the main feeding mouths influence |
| | O5 | | *S. incongruens, L. tumida, Cytheretta* spp., *Aurila* spp., *Semicytherura* spp., *L. napoliana* | 24.2 | 75.8 | 0.5 | 49.6 | Shallower relict sands | Sediment starvation, very sandy substrate with high $CaCO_3$ at moderate water depth |
| | O6 | | *Pontocythere turbida, Semicytherura* spp., *Aurila* spp. | 35.0 | 66.4 | 0.7 | 30.6 | Deeper relict sands | Sediment starvation, sandy substrate at high water depth |
| | O7 | | *C. neapolitana, Semicytherura* spp., *Callistocythere* spp., *Pterigocythereis* spp., *C. edwarsii, Cytheropteron* spp., *Bosquetina* spp. | 34.4 | 32.7 | 0.7 | 32.5 | Fine-grained shelf | Low sediment supply on mixed substrates at high water depth |
| Foraminifers | F1 | | *A. parkinsoniana - A. tepida, N. turgida* | 14.3 | 4.2 | 3.3 | 26.5 | In proximity to the Po and Adige river mouths | High organic matter supply near the main feeding mouths |
| | F2 | | *A. parkinsoniana - A. tepida, A. perlucida, Cribroelphidium ex gr. granosum, Cribroelphidium ex gr. poeyanum* | 16.0 | 13.5 | 0.8 | 29.5 | Along the coast, South of the Po Delta | Moderate organic matter supply at shallow water depth |
| | F3 | | *Q. seminula, Adelosina* spp., *T. trigonula*, other *Quinqueloculina, Cribroelphidium ex gr. granosum, Cribroelphidium ex gr. poeyanum* | 14.5 | 49.7 | 0.6 | 62.0 | Along the coast, North of the Po Delta | Low organic matter supply, strong longshore currents, high $CaCO_3$ at shallow depth updrift of the main feeding sources |
| | F4 | | *N. turgida, V. bradyana* | 30.7 | 2.9 | 1.5 | 28.6 | Mud belt | High organic matter supply south of the feeding mouths at moderate water depth |
| | F5 | | *B. granulata, A. beccarii, A. mamilla, C. lobatulus, N. terquemi, R. bradyi* | 31.6 | 59.7 | 0.6 | 36.8 | Shelf | Low organic matter supply at high water depth |

**Table 2** - List of the modern North Adriatic biofacies defined in Barbieri et al. (2019) through thresholds of environmental variables. Modern biofacies are used in this work as reference for the comparison with fossil assemblages.

| Taxon | Average dissim. | Contribution % | Cumulative % | Mean abundance | | | | | | |
|---|---|---|---|---|---|---|---|---|---|---|
| | | | | TST | | | HST - Volano lobe | | HST - Goro lobe | |
| | | | | 187 S4 | 205 S9 | EM13 | 205 S9 | EM13 | 187 S4 | EM13 |
| *Leptocythere ramosa* | 0.12 | 18.19 | 18.19 | 2.24 | 0.86 | 0.43 | 2.59 | 6.52 | 3.89 | 68.37 |
| *Pontocythere turbida* | 0.07 | 10.75 | 28.95 | 18.99 | 18.05 | 19.71 | 27.32 | 22.43 | 34.72 | 3.86 |
| *Semicytherura incongruens* | 0.06 | 10.09 | 39.04 | 20.44 | 30.59 | 24.95 | 15.18 | 16.68 | 15.08 | 2.73 |
| *Loxoconcha* ex gr. *rhomboidea* | 0.05 | 7.55 | 46.59 | 14.52 | 10.67 | 17.86 | 1.65 | 3.22 | 5.44 | 0.00 |
| *Palmoconcha turbida* | 0.04 | 6.81 | 53.39 | 1.92 | 1.62 | 1.48 | 10.91 | 9.98 | 9.27 | 11.71 |
| Other *Semicytherura* | 0.04 | 5.50 | 58.89 | 13.85 | 14.76 | 15.06 | 7.23 | 7.05 | 5.37 | 0.24 |
| *Sagmatocythere versicolor* | 0.03 | 5.25 | 64.14 | 2.24 | 2.59 | 1.07 | 3.41 | 7.46 | 2.46 | 0.00 |
| *Sagmatocythere napoliana* | 0.03 | 4.34 | 68.48 | 2.24 | 3.63 | 9.94 | 0.31 | 1.83 | 0.00 | 0.00 |
| *Xestoleberis* spp. | 0.03 | 4.04 | 72.52 | 1.76 | 1.44 | 0.41 | 3.38 | 3.96 | 6.33 | 2.15 |
| *Hiltermannicythere turbida* | 0.02 | 3.60 | 76.11 | 1.76 | 5.71 | 1.00 | 0.31 | 0.32 | 0.54 | 7.51 |
| *Hiltermannicythere sphaerulolineata* | 0.02 | 3.49 | 79.60 | 2.40 | 0.81 | 1.09 | 5.33 | 3.82 | 3.93 | 0.86 |
| *Neocytherideis subulata* | 0.02 | 3.10 | 82.70 | 0.00 | 0.52 | 0.36 | 3.87 | 2.52 | 2.66 | 1.25 |
| *Carinocythereis whitei* | 0.02 | 2.88 | 85.58 | 0.79 | 1.33 | 0.34 | 3.53 | 0.87 | 1.02 | 0.45 |
| *Leptocythere bacescoi* | 0.02 | 2.69 | 88.27 | 0.48 | 2.01 | 0.00 | 2.31 | 2.27 | 1.97 | 0.00 |
| *Loxoconcha rubritincta* | 0.01 | 2.25 | 90.53 | 0.96 | 1.04 | 0.00 | 1.86 | 0.00 | 1.41 | 0.00 |
| *Loxoconcha* aff. *L. bonaducei* | 0.01 | 2.01 | 92.54 | 0.48 | 0.00 | 1.43 | 0.97 | 1.78 | 0.08 | 0.00 |
| *Callistocythere* spp. | 0.01 | 1.84 | 94.37 | 1.59 | 1.62 | 0.70 | 0.76 | 0.35 | 1.94 | 0.00 |
| *Cytheretta* spp. | 0.01 | 1.71 | 96.08 | 7.94 | 0.00 | 0.20 | 0.44 | 0.00 | 0.00 | 0.00 |
| *Hemicytherura* spp. | 0.01 | 1.30 | 97.38 | 0.00 | 0.29 | 0.00 | 0.96 | 0.83 | 0.33 | 0.00 |
| Other *Leptocythere* | 0.01 | 0.80 | 98.19 | 0.00 | 0.00 | 0.24 | 0.31 | 0.87 | 0.00 | 0.00 |
| *Pontocypris* spp. | 0.00 | 0.71 | 98.90 | 0.00 | 0.00 | 0.14 | 0.00 | 1.08 | 0.00 | 0.00 |
| *Paracytheridea* spp. | 0.00 | 0.62 | 99.52 | 2.07 | 0.00 | 0.20 | 0.00 | 0.29 | 0.16 | 0.00 |
| *Aurila* spp. | 0.00 | 0.30 | 99.82 | 0.00 | 0.57 | 0.14 | 0.13 | 0.00 | 0.11 | 0.00 |
| *Bosquetina* group | 0.00 | 0.13 | 99.95 | 0.00 | 0.00 | 0.22 | 0.00 | 0.11 | 0.00 | 0.00 |
| *Cytheridea neapolitana* | 0.00 | 0.05 | 100.00 | 0.00 | 0.29 | 0.00 | 0.00 | 0.00 | 0.00 | 0.00 |

**Table 3** - Results of the SIMPER analyses performed on sediment units within each core, on Hellinger-transformed ostracod data, with mean abundances expressed in percentage form. Grey cells evidence characteristic mean frequencies of taxa with a marked paleoecological significance for each study interval. Overall average dissimilarity: 0.64.

804

| | | Core | **Ostracods** | **Foraminifers** |
|---|---|---|---|---|
| **TST** | | 205S9 | 100.0% | 100.0% |
| | | EM13 | 81.3% | 100.0% |
| | | 187S4 | 100.0% | 100.0% |
| **HST** | **Volano lobe** | 205S9 | 25.0% | 90.6% |
| | | EM13 | 38.9% | 55.7% |
| | **Goro lobe** | 187S4 | 69.0% | 93.8% |
| | | EM13 | 6.0% | 100.0% |

805

806 **Table 4** - Relative abundance of significant modern analogs per unit based on the four most similar modern

807 sites.

808

| Taxon | Average dissim. | Contribution % | Cumulative % | Mean abundance | | | | | | |
|---|---|---|---|---|---|---|---|---|---|---|
| | | | | TST | | | HST - Volano lobe | | HST - Goro lobe | |
| | | | | 187 S4 | 205 S9 | EM13 | 205 S9 | EM13 | 187 S4 | EM13 |
| *Ammonia parkinsoniana - A. tepida* | 0.11 | 25.85 | 25.85 | 15.61 | 11.42 | 3.94 | 57.49 | 36.50 | 63.67 | 62.73 |
| *Aubignyna perlucida* | 0.03 | 8.07 | 33.92 | 2.82 | 1.28 | 0.00 | 6.59 | 11.09 | 5.98 | 17.21 |
| *Quinqueloculina* group | 0.03 | 7.62 | 41.54 | 14.11 | 15.82 | 17.34 | 4.91 | 8.05 | 4.61 | 1.03 |
| *Porosononion* ex gr. *granosum* | 0.03 | 7.41 | 48.95 | 10.68 | 13.76 | 12.54 | 3.56 | 10.49 | 3.49 | 9.22 |
| *Triloculina* ex gr. *trigonula* | 0.03 | 6.73 | 55.68 | 5.56 | 8.44 | 14.20 | 1.00 | 3.95 | 1.71 | 0.16 |
| *Nonionella turgida* | 0.02 | 5.50 | 61.17 | 0.90 | 1.59 | 0.40 | 1.99 | 4.55 | 1.10 | 0.17 |
| *Ammonia beccarii* | 0.02 | 4.90 | 66.07 | 1.51 | 3.81 | 2.32 | 3.78 | 0.44 | 1.04 | 1.00 |
| *Textularia agglutinans* | 0.02 | 4.76 | 70.83 | 8.03 | 4.54 | 4.75 | 1.06 | 1.88 | 0.77 | 0.00 |
| *Haynesina* spp. | 0.02 | 4.76 | 75.60 | 2.37 | 3.03 | 0.47 | 6.37 | 3.44 | 6.16 | 1.29 |
| *Adelosina* spp. | 0.02 | 4.00 | 79.60 | 9.79 | 7.26 | 6.74 | 1.89 | 3.33 | 1.89 | 1.15 |
| *Cribroelphidium* ex gr. *poeyanum* | 0.01 | 3.29 | 82.89 | 7.29 | 5.08 | 2.81 | 3.91 | 2.04 | 4.06 | 3.31 |
| *Elphidium advenum* | 0.01 | 2.86 | 85.75 | 4.59 | 5.81 | 2.50 | 1.31 | 1.07 | 0.66 | 0.09 |
| *Asterigerinata mamilla* | 0.01 | 2.66 | 88.40 | 0.00 | 0.00 | 3.66 | 0.00 | 1.52 | 0.00 | 0.00 |
| *Rosalina bradyi* | 0.01 | 2.53 | 90.93 | 2.55 | 0.29 | 5.29 | 0.20 | 1.04 | 0.10 | 0.00 |
| *Neoconorbina terquemi* | 0.01 | 2.27 | 93.20 | 0.00 | 0.00 | 5.44 | 0.00 | 0.74 | 0.00 | 0.00 |
| *Buccella granulata* | 0.01 | 2.23 | 95.43 | 1.94 | 2.13 | 6.09 | 0.37 | 0.38 | 0.21 | 0.09 |
| *Quinqueloculina seminula* | 0.01 | 1.88 | 97.31 | 0.74 | 3.29 | 2.68 | 1.39 | 1.58 | 1.24 | 2.04 |
| *Elphidium crispum* | 0.01 | 1.37 | 98.68 | 1.79 | 1.50 | 1.24 | 0.41 | 0.23 | 0.19 | 0.00 |
| *Reussella spinulosa* | 0.00 | 0.60 | 99.28 | 0.30 | 0.00 | 0.16 | 0.03 | 0.42 | 0.03 | 0.00 |
| *Cassidulina carinata* | 0.00 | 0.32 | 99.60 | 0.15 | 0.00 | 0.00 | 0.15 | 0.01 | 0.11 | 0.05 |
| *Bulimina marginata* | 0.00 | 0.20 | 99.81 | 0.00 | 0.00 | 0.00 | 0.00 | 0.01 | 0.13 | 0.14 |
| *Cibicidoides lobatulus* | 0.00 | 0.19 | 100.00 | 0.00 | 0.00 | 0.38 | 0.02 | 0.04 | 0.03 | 0.00 |
| *Valvulineria bradyana* | 0.00 | 0.00 | 100.00 | 0.00 | 0.00 | 0.00 | 0.00 | 0.00 | 0.00 | 0.00 |

**Table 5** - Results of the SIMPER analyses performed on sediment units within each core, on Hellinger-transformed benthic foraminiferal data, with mean abundances expressed in percentage form. Grey cells evidence characteristic mean frequencies of taxa with a marked paleoecological significance for each study interval. Overall average dissimilarity: 0.42.

| | | | Ostracods | | | | Benthic foraminifers | | | |
|---|---|---|---|---|---|---|---|---|---|---|
| | | | Water depth (m) | | Sand concentration (%) | | Water depth (m) | | Organic matter (%) | |
| | | | Estimated value | S.E. | Estimated value | S.E. | Estimated value | S.E. | Estimated value | S.E. |
| 205S9 | TST | | 23.3 | 1.1 | 58.3 | 3.5 | 18.4 | 1.3 | 0.8 | 0.3 |
| | HST | Volano prodelta | 15.3 | 1.3 | 35.1 | 3.8 | 13.1 | 1.5 | 2.0 | 0.4 |
| | | Volano delta front | 14.8 | 1.2 | 42.0 | 3.8 | 12.2 | 1.5 | 2.2 | 0.4 |
| EM13 | TST | | 22.3 | 1.2 | 67.9 | 4.1 | 26.0 | 1.3 | 0.6 | 0.4 |
| | HST | Volano prodelta | 15.0 | 1.2 | 31.7 | 3.9 | 14.7 | 1.3 | 1.5 | 0.4 |
| | | Goro prodelta | 14.0 | 1.3 | 3.6 | 4.3 | 12.2 | 1.5 | 2.3 | 0.4 |
| 187S4 | TST | | 20.2 | 1.0 | 62.7 | 3.8 | 17.6 | 1.3 | 0.9 | 0.3 |
| | HST | Goro prodelta | 15.0 | 1.2 | 42.8 | 3.9 | 12.4 | 1.4 | 2.1 | 0.4 |

**Table 6** – Average values of estimated parameters *per* study unit within each core and associated standard error (S.E.), considering only samples represented by significant modern analogs.

821 **Figures**

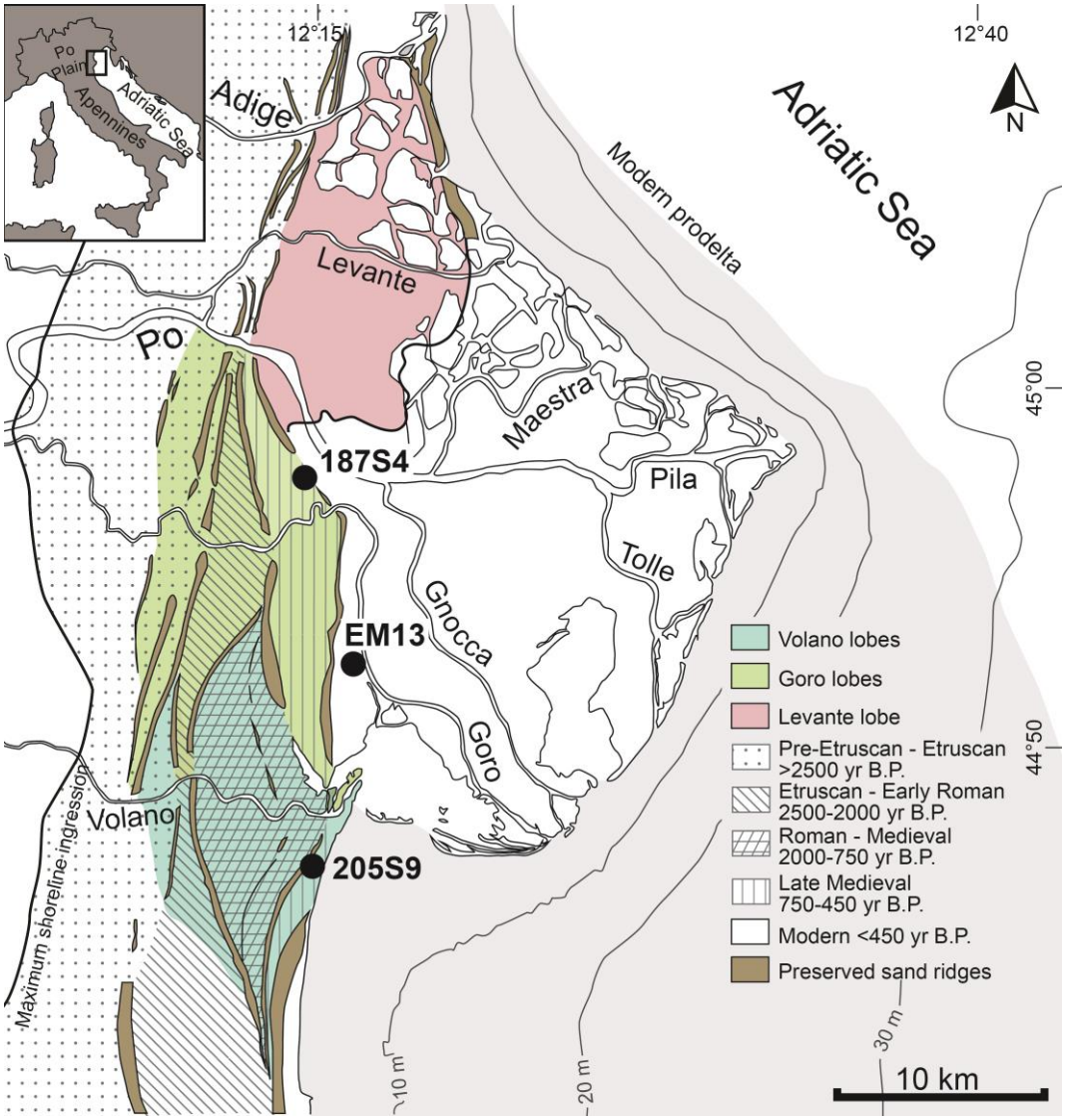


822

823 **Figure 1** – Location of the three study cores and extension of Po Delta lobes based on preserved onshore
824 sand ridges (from Ciabatti, 1967). Maximum shoreline ingression from Bruno et al. (2017), seaward extent of
825 the modern prodelta from Correggiari et al. (2005a).

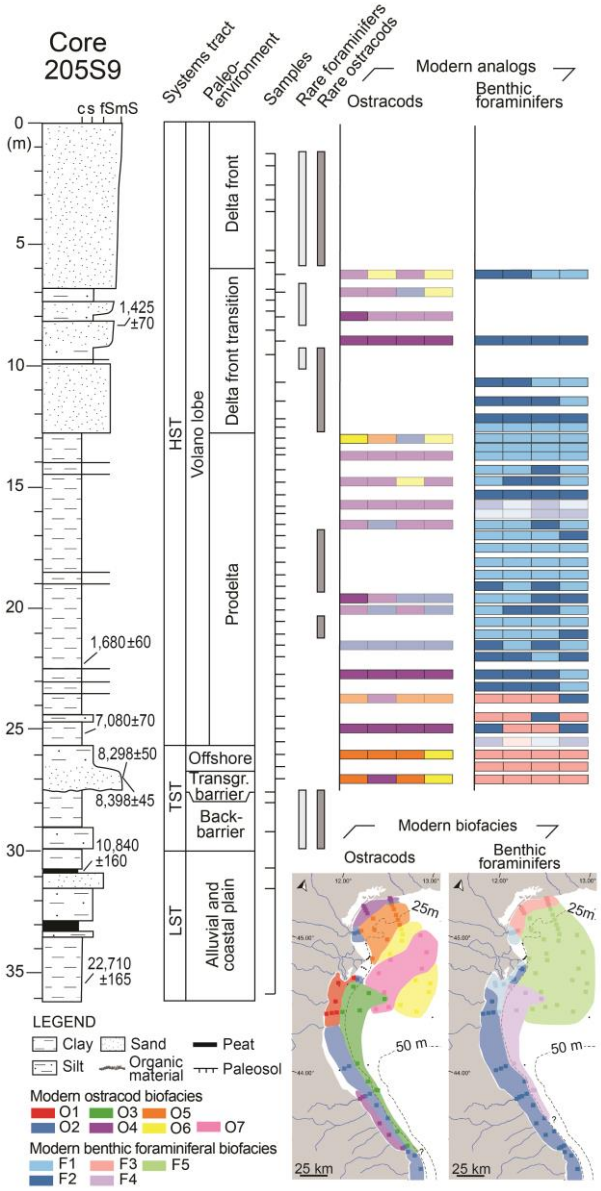


826

827 **Figure 2** – Stratigraphy and modern analogs for benthic ostracods and foraminifers of core 205S9. On the
828 right of the stratigraphic log, ages are reported as calibrated years B.P. Samples included in multivariate
829 ordinations on the right of the sample column; on the left, samples inspected for quantitative analyses, but
830 including a poor fauna. Significant modern analogs are reported in bold colors, whereas non-significant
831 analogs, up to the fourth most similar sample, are reported in shaded tones. Colors are in accordance with
832 modern biofacies defined in Barbieri et al. (2019), whose distribution is reported on the bottom of the figure.

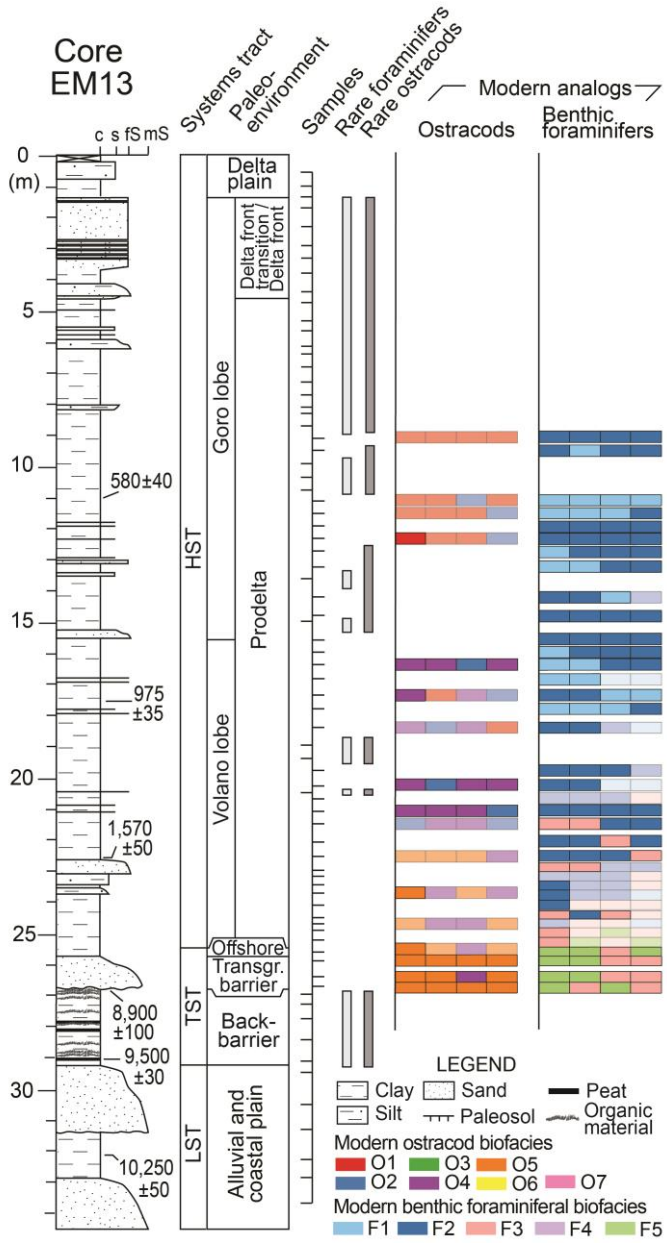


833

834 **Figure 3** - Stratigraphy and modern analogs for benthic ostracods and foraminifers of core EM13. On the

835 right of the stratigraphic log, ages are reported as calibrated years B.P. For additional information, including the

836 distribution of the modern biofacies, the reader is invited to refer to Fig. 2.

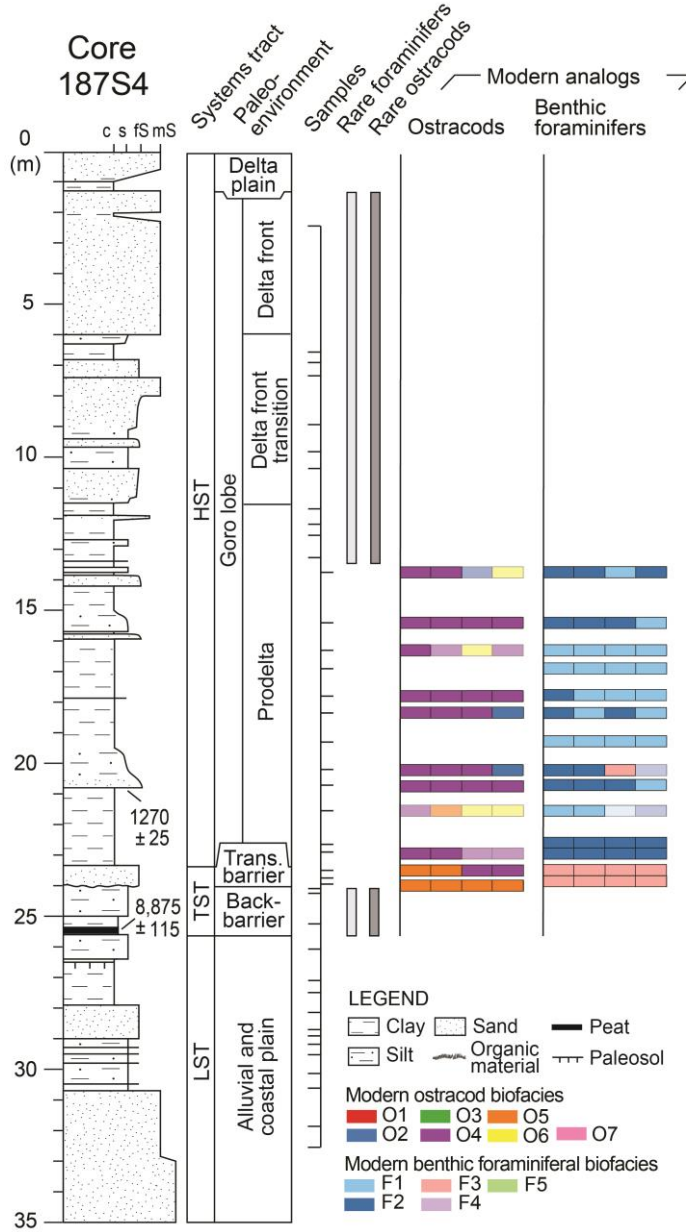


837

838 **Figure 4** - Stratigraphy and modern analogs for benthic ostracods and foraminifers of core 187S4. On the

839 right of the stratigraphic log, ages are reported as calibrated years B.P. For additional information, including the

840 distribution of the modern biofacies, the reader is invited to refer to Fig. 2.

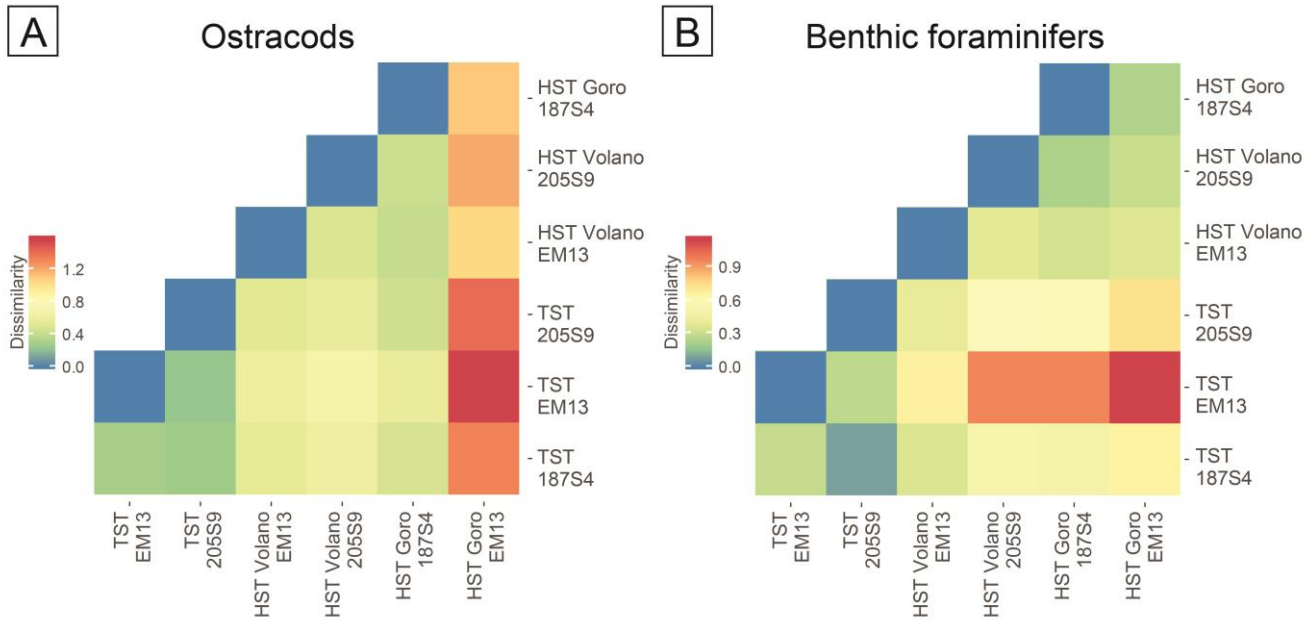


841

842 **Figure 5** – Graphic display of benthic ostracod (a) and foraminifer (b) dissimilarity matrices for transgressive

843 and highstand units of the Volano and Goro lobe in each core.

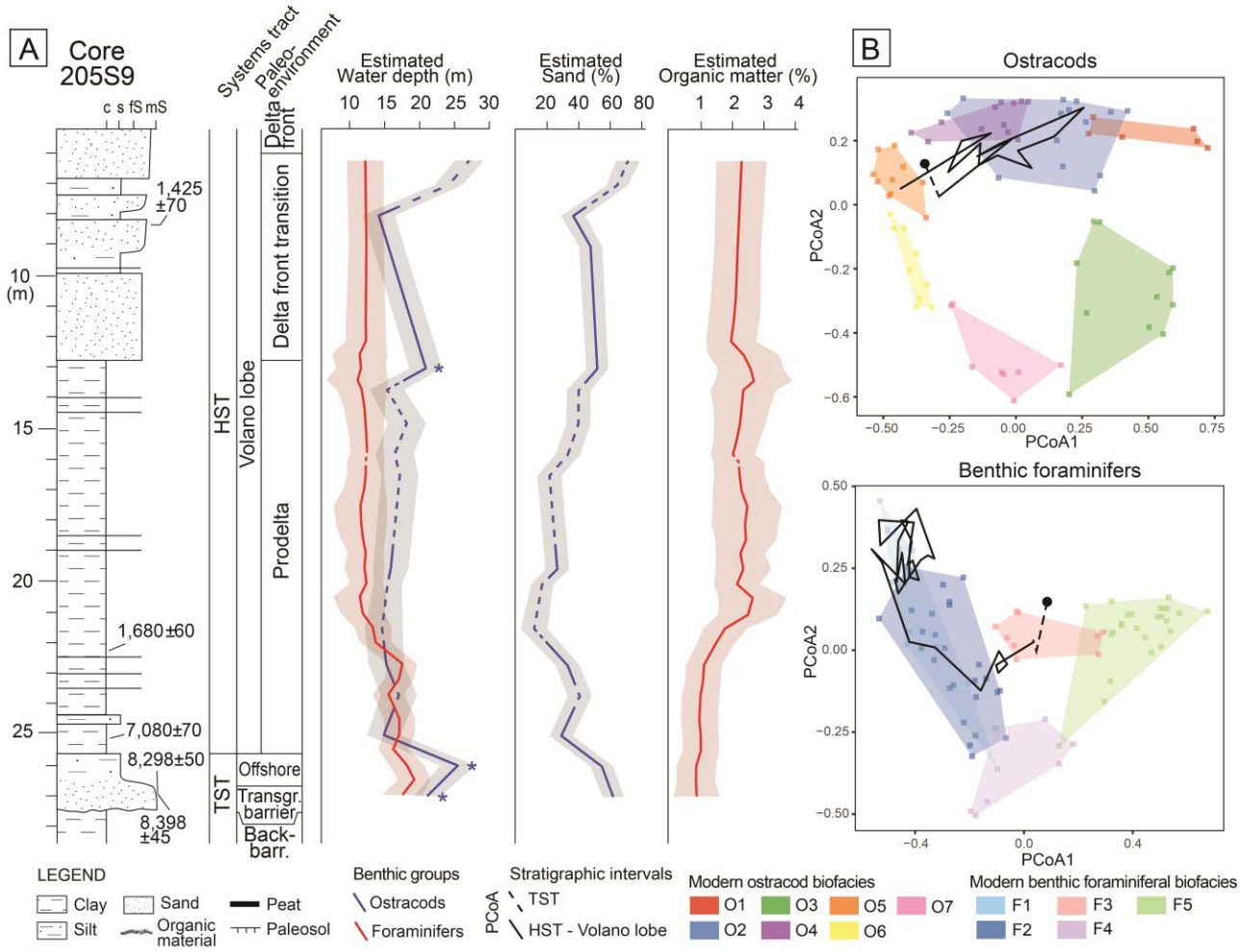


844

845 **Figure 6** – (a) Estimated values of environmental drivers on the modern benthic ostracods and foraminifers
846 (from Barbieri et al., 2019) extracted from the wPCoA of core 205S9. Estimated abiotic values that do not
847 reflect true modern environmental conditions are marked by asterisks. Dashed lines indicate estimated values
848 from samples with no significant modern analogs. On the right of the stratigraphic log, ages are reported as
849 calibrated years B.P. (b) In the wPCoA, the core trajectory is indicated by a black line starting from a point and
850 partitioned into study units. The core trajectory is superimposed over the distribution of modern sites on the
851 multivariate space, grouped in accordance to modern biofacies.

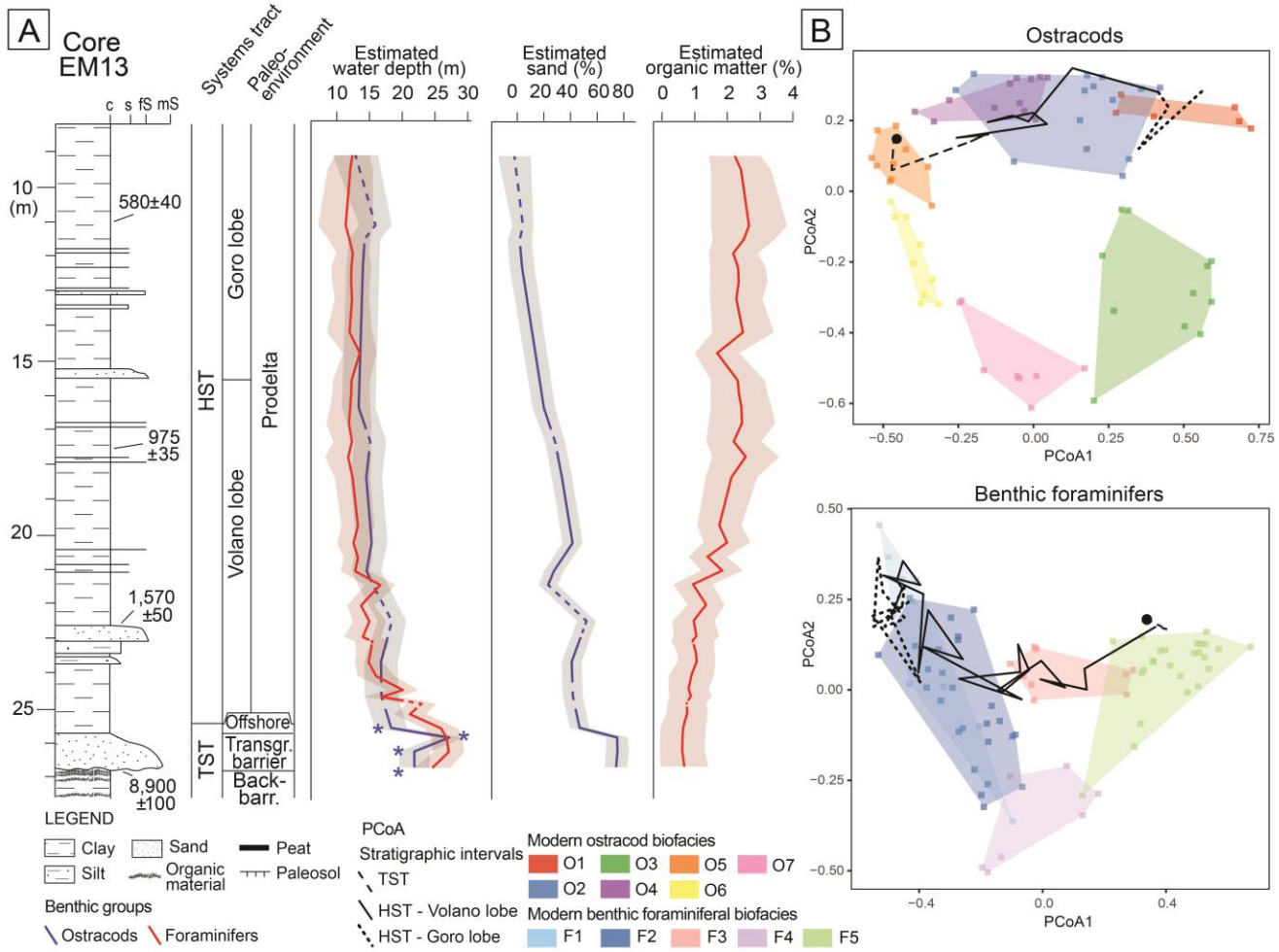


852

853 **Figure 7** – (a) Estimated values of environmental drivers on the modern benthic ostracods and foraminifers
854 (from Barbieri et al., 2019) extracted from the wPCoA of core EM13. On the right of the stratigraphic log, ages
855 are reported as calibrated years B.P. (b) wPCoA of the core trajectory superimposed over the distribution of
856 modern sites on the multivariate space, grouped in accordance to modern biofacies. For further explanations,
857 refer to Figure 6.

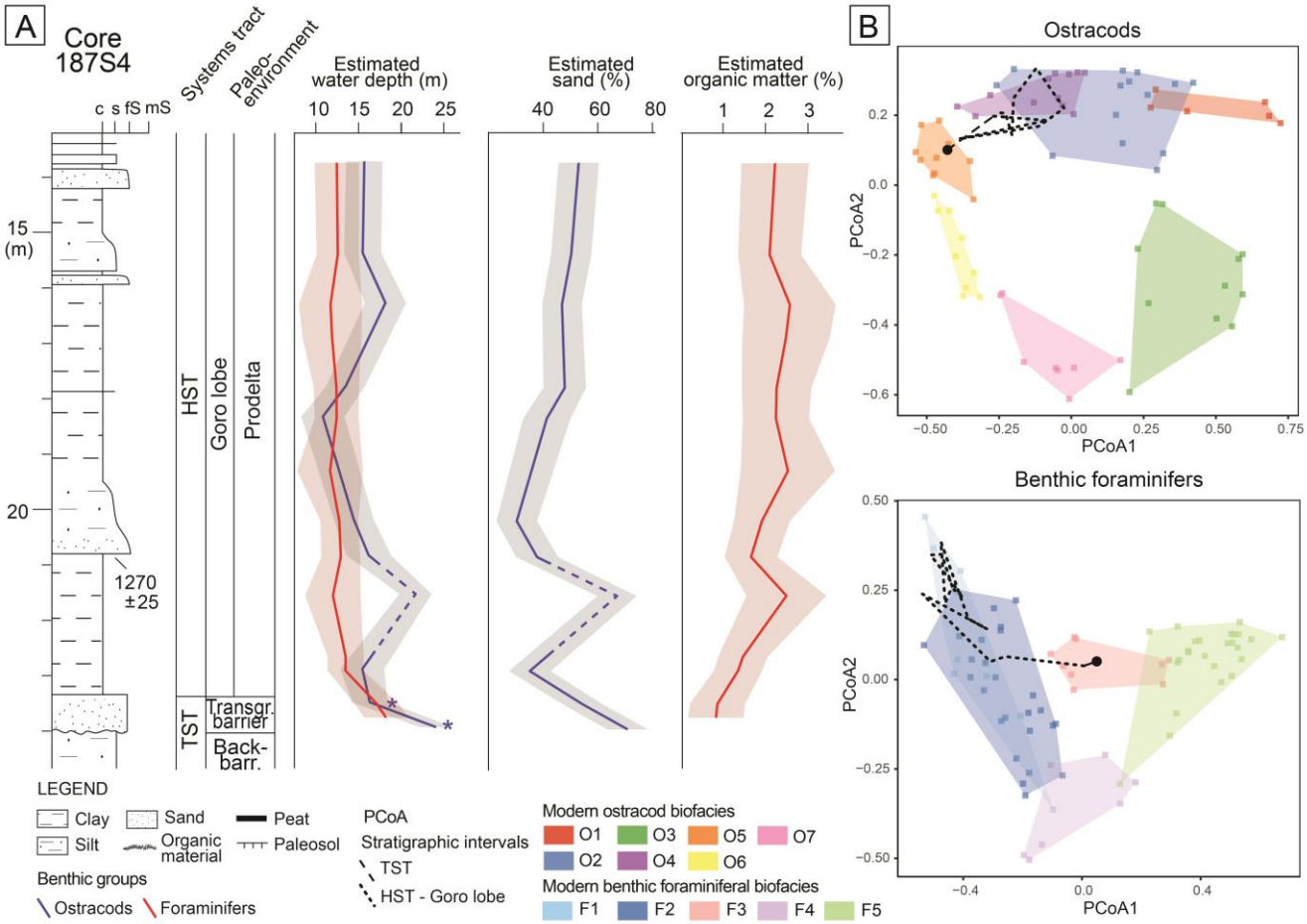


858

859 **Figure 8** – (a) Estimated values of environmental drivers on the modern benthic ostracods and foraminifers
860 (from Barbieri et al., 2019) extracted from the wPCoA of core 187S4. On the right of the stratigraphic log, ages
861 are reported as calibrated years B.P. (b) wPCoA of the core trajectory superimposed over the distribution of
862 modern sites on the multivariate space, grouped in accordance to modern biofacies. For further explanations,
863 refer to Figure 6.

864

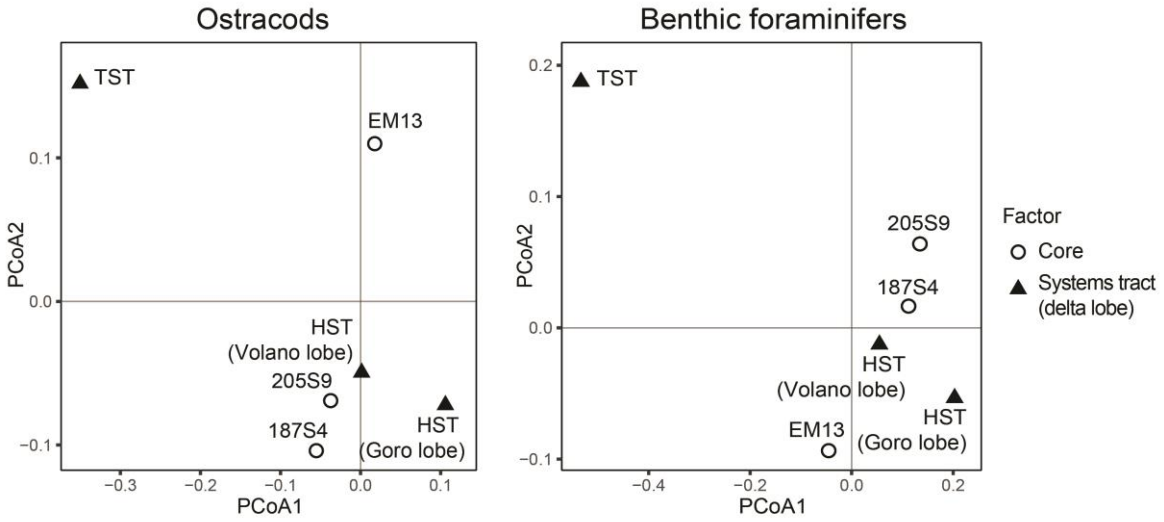


865

866 **Figure 9** – PCoA ordination of distances among the centroids for individual levels of the two main effects in
867 the benthic ostracod (a) and foraminifer (b) dataset, namely cores (205S9, EM13, 187S4) and systems tracts
868 (transgressive and highstand Volano and Goro delta lobe deposits).